On the occurrence of baddeleyite in zircon in silica-saturated rocks

Alexander Lewerentz

Bachelors thesis in Geology at Lund University - Lithosphere and Paleobiosphere Sciences, no. 261 (15 hskp/ECTS)

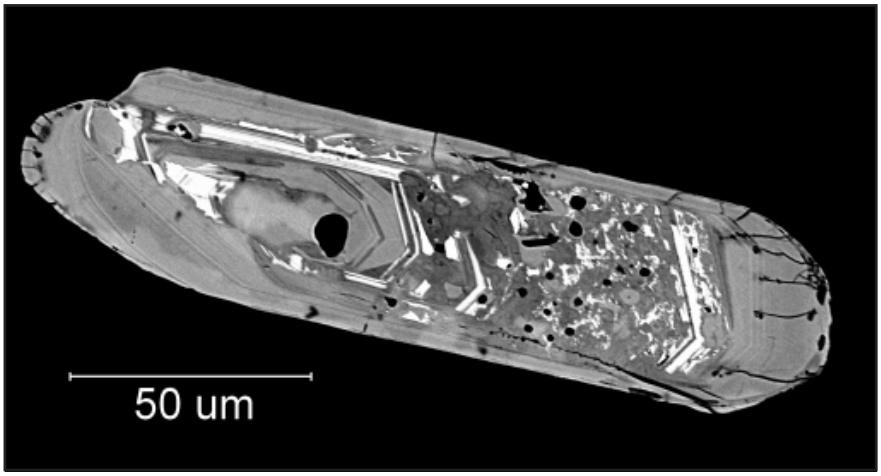

Department of Earth- and Ecosystem Sciences
Division of Geology
Lund University

2010

On the occurrence of baddeleyite in zircon in silica-saturated rocks

Bachelor Thesis
Alexander Lewerentz

Department of Earth and Ecosystem Sciences
Lund University
2010

Contents

1 Introduction **5**
2.1 Background 5
2.2 Regional Geology 5
2.3 Samples 5
2 Methods **7**
2.1 Light microscopy 7
2.2 Scanning electron microscopy 7
2.2.1 BSE 7
2.2.2 CL 7
2.2.3 EDS 7
3 Results **7**
3.1 Light microscopy 7
3.1.1 Thin section 468720b 7
3.1.2 Thin section 508602 7
3.1.3 Thin section 510155 9
3.1.4 Thin section 512013 9
3.1.5 Thin section 512028 9
3.1.6 Thin section 512075 9
3.2 SEM-EDS 12
3.2.1 Zircon mount 510155 12
3.2.2 Zircon mount 512028 12
3.2.3 Thin section 468720 16
3.2.4 Thin section 510155 19
3.2.5 Thin section 512028 21
3.2.6 Thin section 512075 21
3.3 Geochemistry 23
4 Discussion **23**
4.1 Zircon occurrence 23
4.2 SEM-EDS 24
4.3 Primary or secondary processes? 24
4.4 Possible explanations 24
5 What next? **24**
6 Conclusions **25**
7 Acknowledgements **25**
8 References **25**
Appendix 1: Thin section overviews **26**
Appendix 2: Photos of zircon grains in thin section **32**
Appendix 3: EDS-data **38**
Appendix 4: EDS line scans **45**
Appendix 5: Geochemical data **54**

Cover Picture: A baddeleyite bearing zircon grain from zircon mount for sample 512028, in the thesis mentioned as zircon area 8.

On the occurrence of baddeleyite in zircon in silica-saturated rocks

ALEXANDER LEWERENTZ

Lewerentz, A., 2010: On the occurrence of baddeleyite in zircon in silica-saturated rocks. *Examensarbeten i geologi vid Lunds universitet*, Nr. XX, 54 pp. 15 hskp (15 ECTS credits).

Abstract: Baddeleyite (ZrO_2) is an important mineral for U-Pb geochronology in silica undersaturated rocks. Under silica saturated conditions, baddeleyite reacts to form zircon. Yet, I document baddeleyite domains within zircon in several silica-saturated rock types. The primary aim of this project is to describe the phenomenon in detail. To reach this aim polarisation microscopy and SEM-EDS analyses have been used. Based on the descriptions, possible models for the origin of the phenomenon are suggested, including both primary and secondary processes. I suggest that variations in the silica-activity might explain the occurrence of possible primary baddeleyite bands, and that later hydrothermal processes are responsible for the formation of baddeleyite in alteration processes. Suggestions on further analyses are also presented.

Keywords: zircon, baddeleyite, silica-saturated rocks, scanning electron microscopy, energy dispersive x-ray spectroscopy

Alexander Lewerentz, Department of Earth & Ecosystem Sciences, Lund University, Sölvegatan 12, 223 62 Lund, Sweden. E-mail: alexander.lewerentz@gmail.com

Om förekomsten av baddeleyit i zirkon i kiselmättade bergarter

ALEXANDER LEWERENTZ

Lewerentz, A., 2010: On the occurrence of baddeleyite in zircon in silica-saturated rocks. *Examensarbeten i geologi vid Lunds universitet*, Nr. X, 54 sid. 15 hskp (15 ECTS credits).

Sammanfattning: Baddeleyit (ZrO_2) är ett viktigt mineral för U-Pb-geokronologi i kiselundermättade bergarter. Vid kiselövermättade förhållanden reagerar baddeleyit med kvarts för att bilda zirkon. Trots detta beskriver jag i denna uppsats baddeleyitdomäner inuti zirkoner från ett flertal kiselsövermättade bergarter. Det primära målet med det här projektet är att beskriva fenomenet i detalj. För att göra detta har polarisationsmikroskopi och svepelektronmikroskopi (inklusive röntgenemissionspektroskopi) använts. Med beskrivningarna som stöd föreslås möjliga modeller för fenomenets ursprung. Dessa modeller innefattar både primära och sekundära processer. Som primär process föreslås variationer i kiselaktivitet och som sekundär hydrotermal omvandling. Avslutningsvis presenteras förslag på framtida undersökningar.

Nyckelord: zirkon, baddeleyit, kiselmättade bergarter, svepelektronmikroskopi, röntgenemmissionspektroskopi

Alexander Lewerentz, Institutionen för geo- och ekosystemvetenskaper, Lunds Universitet, Sölvegatan 12, 223 62 Lund, Sverige. E-post: alexander.lewerentz@gmail.com

1 Introduction

1.1 Background

Baddeleyite (ZrO_2) is an important mineral for U-Pb geochronology in silica undersaturated rocks. Under silica saturated conditions, baddeleyite reacts to form zircon along the reaction:

$$ZrO_2 + SiO_2 \rightleftharpoons ZrSiO_4 \quad \text{[Eq. 1]}$$

Yet, I document baddeleyite domains within zircon in several quartz-saturated rock types from southern West Greenland. In order to explain the observations of baddeleyite are documented in zircon derived from granite, felsic pegmatite and possibly metasedimentary rocks; the primary aim of this project is to make detailed petrographical and textural descriptions of the phenomenon. In this manner we hope to better understand the origin of baddeleyite. Is the baddeleyite of primary magmatic origin, or an effect of secondary alteration, i.e. can the baddeleyite to zircon reaction be reversed (Eq. 1)? Is there any link to regional geology or to the presence of detrital baddeleyite grains?

1.2 Regional geology

A majority of the Greenlandic shield was originally occupied by the Archaean basement, but only the southern part of the shield escaped Post-Archaean orogenic events. In Central to North Greenland, the basement was reworked between 2000 Ma and 1750 Ma and stabilisation of the Greenlandic shield took place between 1750 Ma and 1600 Ma (Henriksen 2008).

The craton of southern West Greenland is made up of six crustal blocks; the Maniitsoq, Fiskefjord, Sermilik, Bjørnesund, Kvanefjord and Ivittuut blocks (Windley & Garde 2009). These blocks are constructed of numerous terranes (Friend et al. 1996). The different blocks were created in island arc and active continental margin arc settings. Since the blocks are slightly tilted, the recent surface represent both lower and upper crustal zone of the original Archaean craton. The upper crustal zone consists of prograde amphibolite metamorphic facies rocks, whilst the lower crustal zone consists of retrograde amphibolite and granulite facies metamorphic rocks (Windley & Garde 2009).

The accretion of the terranes in southern Western Greeland is believed to have occurred in two main events. The first event is dated to ~2.99-2.95 Ga (Friend & Nutman 2005). This event may have involved the Isukasia, Kapisilik and Akia terranes (Hanmer et al. 2002; Friend & Nutman 2005). Granites mainly intruding the Sermilik block, but also occurring as satellite intrusions in the Bjørnesund block, have been dated to ~2.8 Ga (Ilivertalik granite). This implies that these two blocks were a single unit by 2.8 Ga (Keulen et al. 2009). The second event is thought to have taken place at approximately 2.73-2.71 Ga. This event includes minor granite emplacement from a continental crust source. These granites are associated with amphibolite facies metamorphism, of the same time period (Friend et al. 1996).

Tonalite-trondhjemite-granodiorite-type (TTG) gneisses are representing the main crust-generating period. These gneisses have intrusive ages of 2.92 Ga to 2.84 Ga (Schiøtte et al. 1989; Næraa & Scherstén 2008). Several granite complexes are present and the most important granite in this area is the Ilivertalik augen granite, dated to 2.8 Ga (Pidgeon & Kalsbeek 1978). In addition garnet or sillimanite bearing mica schists are common throughout the area (Keulen et al. 2009).

The Bjørnesund block extends from the Fredrikshåb Isblink, northwards to just south of the Grædefjord. Approximately half of the recent surface of the block is represented by lower crustal zone rocks. Subsequently, the other half is represented by upper crustal zone rocks. The lower crustal zone is present in the north half of the block, and the upper crustal zone in the south half of the block (Windley & Garde 2009). Further, several amphibolite belts are present, e.g. the Ikkattup Nunaa belt and at Majoqqap Qaava. Majoqqap Qaava is part of the Fiskenæsset anorthosite complex. It has been established that the two earlier mentioned examples of amphibolite belts share a common origin. This origin has been proposed to be a convergent margin setting (Keulen et al. 2009), with an age of 2.91 ± 0.01 Ga (Nutman et al. 2004).

The Sermilik block is situated north of the Bjørnesund block, extending from Grædefjord in the south to Buksefjorden and Ameralik fjord in the north. The whole block is folded in an antiform and therefore lower crustal zone rocks occur in the middle of the block. This zone is then surrounded by a thin layer of upper crustal zone rocks, present in the northern-most and southern-most parts of the block (Windley & Garde 2009).

1.3 Samples

The following rocks, from the Bjørnesund and Sermilik blocks, are included in this study (Figure 1).

468720
The Tre Brødre mica schist, a rock mapped as garnet-sillimanite-biotite schist. It is possibly a metasediment, metamorphosed to amphibolite facies.

508602
A rock mapped as quartz-rich anthophyllite-garnet-plagioclase gneiss and in field interpreted as wallrock to a cataclastic fault zone.

510155
The Nukagpiarssuaq (NGI) granite.

512013
A gneissic metasediment, mapped as Ilivertalik granite.

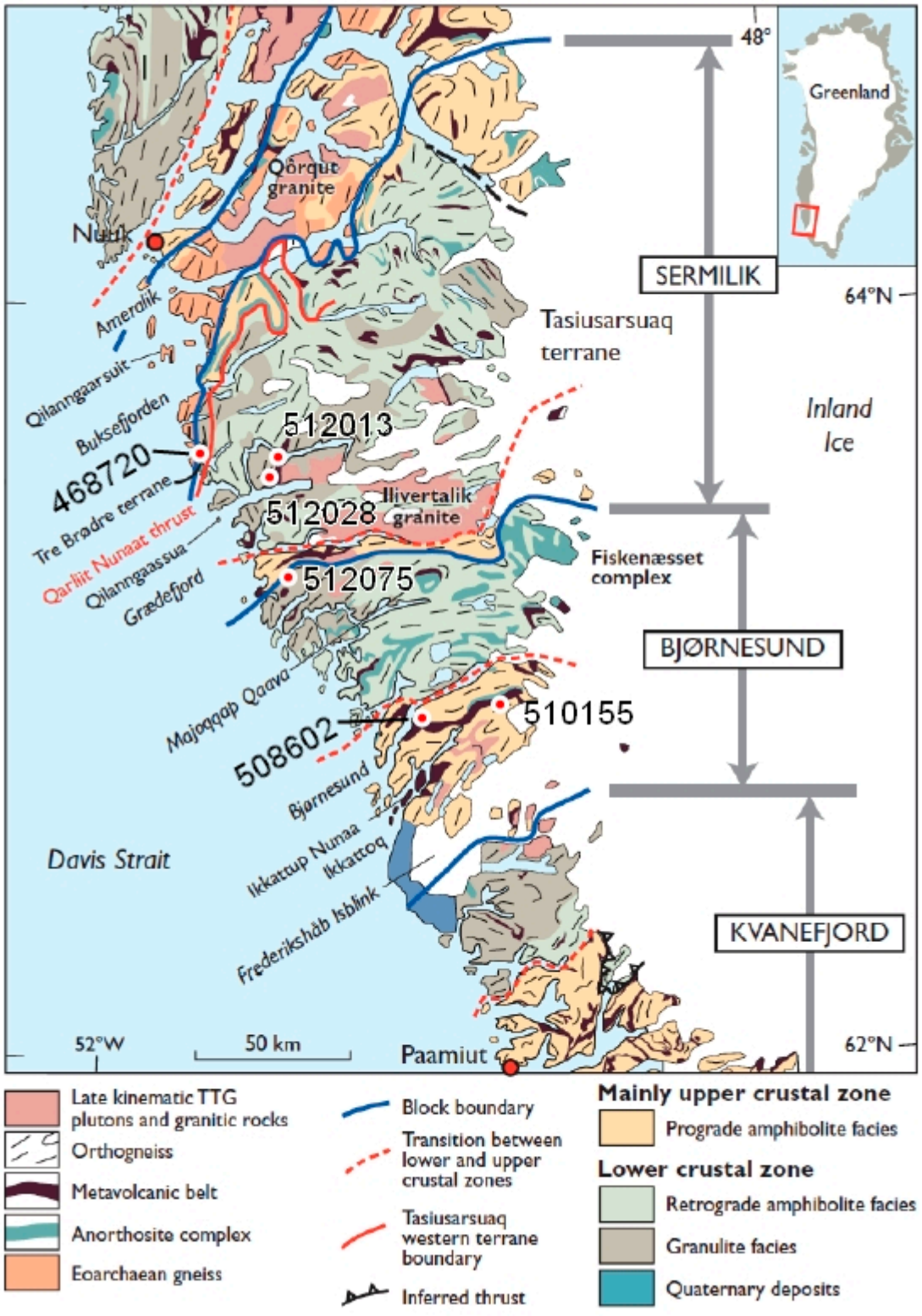

Figure 1: A map over southern West Greenland. All samples included in this study are marked with red spots (modified from Keulen et al. 2009).

512028
A pegmatite from the Sermilik block.

512075
A pegmatite from the Grædefjord shear zone.

2 Methods

2.1 Polarisation microscopy

Thin sections from all samples were studied under polarisation microscope. Descriptions were made in terms of mineralogy, texture, structures and metamorphism. The primary objective was to establish the textural context in which zircon occurs. Examples of zircon occurrences were documented using a ocular camera (Appendix 2). An overview was made of each thin section, using an image scanner. All zircon occurrences identified under the microscope was plotted in these overviews (Appendix 1).

2.2 Scanning electron microscopy

2.2.1 BSE

Scanning electron microscopy (SEM) images are obtained during scanning of an electron beam hitting the surface a the sample. In this study Back scatter electron (BSE) mode is used and therefore explained in more detail below (Reed 1995).

All samples studied using SEM-BSE were coated by a thin layer (~25 nm) of carbon.

The SEM-BSE signal is obtained by the measurement of electrons, derived from the incident beam, that have suffered large deflection within the sample and re-emerged from the surface. Contrast in BSE-images is dependent of the atomic number of the sample, or mean atomic number if the sample is a compound (Reed 1995), i.e. the contrast will show the difference in density between compounds within an image. A less dense compound will appear darker than a more dense.

2.2.2 CL

A Cathode luminescence (CL) picture is obtained by imaging of the light emitted during electron bombardment of the sample. This light is almost only produced by trace elements, such as manganese and the rare earth elements (Long 1995), i.e. CL reflects compositional contrasts.

2.2.3 EDS

Energy Dispersive X-ray Spectroscopy (EDS) is an analytical technique with many applications. It is often used together with the SEM technique. On a broad scale it works as follows. When the electron beam hits the sample, X-ray radiation is emitted. The radiation is measured with an EDS detector and the various energy values are then sorted into 20 eV wide channels. The results are displayed as a spectrum with a number of peaks (spectral lines). This spectrum depends on the composition of the analysed spot. In a spectrum, all elements have several peaks, depending on the emitting energy level. The various peaks are then compared with a known mineral standard to establish the composition of the analysed spot (Champness 1995). This comparison involves corrections for atomic number, absorption and fluorescence (ZAF-corrections). It is done using synthetic or natural mineral standard for all elements. The standards have been measured in the same way as the unknown sample.

To make quantitative analyses a calibration of the microscope is needed. In the used instrument (Oxford INCA system), this is done by analysing a cobalt standard. The calibration associates a specific count rate for any channel with the settings of the SEM. This calibration has been performed for both sample and mineral standards, which makes it possible to compare the analysed sample with the mineral standard.

Two EDS-techniques were used to analyse the samples. Spot analyser was used to quantitatively analyse the composition in a spot (Appendix 3). To calculate the composition a cobalt standard was used. Line mapping was used to establish the relative abundance of different elements along a line, presented as counts per seconds and length interval (Figure 4 and Appendix 4).

3 Results

3.1 Light microscopy

3.1.1 Thin section 468720

Minerals identified and amounts estimated; quartz (65 %), sillimanite (15 %), biotite (10 %), k-feldspar (5 %), garnet (<5 %), muscovite (<5 %) and plagioclase (<5 %). Accessory minerals identified were apatite and zircon (Figure 2).

This rock shows fine to medium inhomogeneous grain size. Garnet is fractured and these fractures are filled with biotite.

Zircon is mostly associated with biotite (8), but a couple of grains also occurs in quartz. A total of ten zircon grains were observed.

In this rock a foliation is present. It is defined by prominent bands of biotite, sillimanite and muscovite, but can also be seen as elongation of larger quartz grains. Biotite, muscovite and sillimanite are concentrated to the foliation planes, though biotite and sillimanite occur much less abundant outside the planes as well. Sillimanite commonly occurs as fibrolite associated with muscovite and muscovite-sillimanite intergrowth can be observed as stripy needle bundles within the foliation bands. Highly abundant micro fractures, cross-cutting the foliation at discordance of ~120° (and occasionally ~60°), are present in the rock. In quartz, grain boundary migration is observed, mostly as bulging but also as nucleation. Some examples of dislocation migration are also observed.

3.1.2 Thin section 508602

Minerals were identified and amounts estimated as following; quartz (50 %), anthophyllite (20 %), plagioclase (20 %), biotite (5 %), garnet (<5 %), opaque (<5

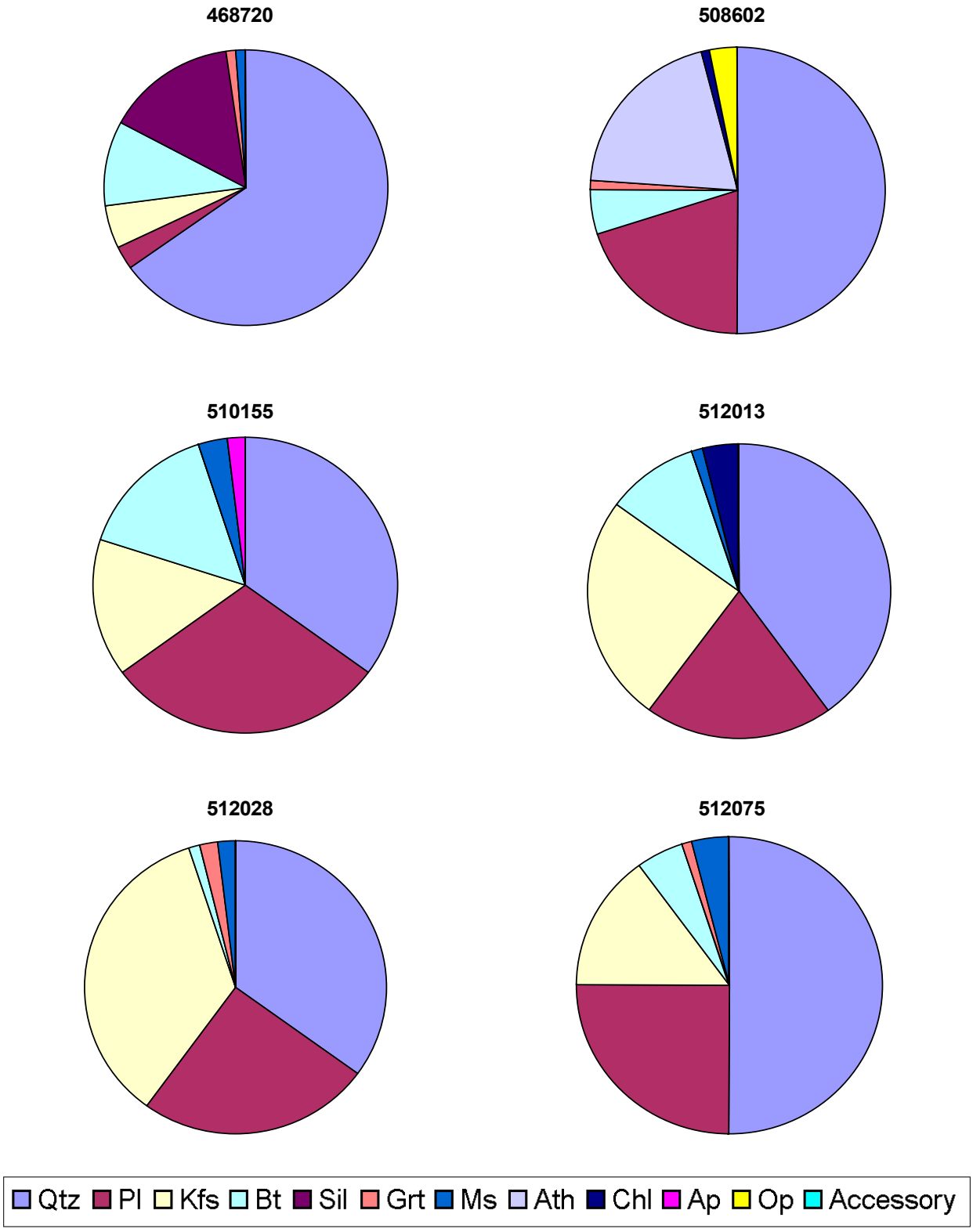

Figure 2: Circle charts showing mineral compositions (in %) for all studied thin sections. Mineral abbreviations follow standard nomenclature as follows: Qtz: quartz, Pl: plagioclase, Kfs: K-feldspar, Bt: biotite, Sil: sillimanite, Grt: garnet, Ms: muscovite, Ath: anthophyllite, Chl: chlorite, Ap: apatite, Op: opaque minerals, Accessory minerals, e.g. zircon.

%) and chlorite (<5 %). Accessory minerals identified were zircon, hematite and titanite (Figure 2).

This rock is homogeneously fine grained, with the exception of a few larger garnet grains. The garnet is partly replaced by an unknown mineral. Grain triple junctions mostly show angles around 120°. Biotite is commonly chloritizised. Hematite occurs as small flakes (thin enough to be non-opaque). Titanite grains are small, anhedral and showing a disturbed appearance.

Three zircon grains were observed in this thin section, two associated with plagioclase and one with quartz. In addition, metamict zircon grains were observed.

Sub-parallel veins with unknown filling occur throughout the thin section.

3.1.3 Thin section 510155

In this rock the following minerals were observed and their amounts estimated; quartz (35 %), plagioclase (30 %), K-feldspar (15 %), biotite (15 %), muscovite (<5 %), apatite (<5 %). Zircon, hematite, opaque and possibly allanite are present as accessory minerals (Figure 2).

The rock is mainly of medium grain size. Though, it is inhomogeneous and smaller grains of all major minerals are present. Apatite and muscovite only occur as fine grains. Hematite is observed as small flake (thin enough to be non-opaque). Some of the plagioclase and K-feldspar grains leave a deformed or altered appearance. In some of the apatite grains smaller grains are present as inclusions. Radiating fractures are centring from these smaller grains, a feature commonly associated with allanite. Some cases of plagioclase-quartz intergrowth (myrmekite) have been observed.

Over 40 zircon grains were observed in this thin section, mostly associated with biotite. In addition a large number of zircon grains are associated with quartz and a few each associated with plagioclase, K-feldspar and apatite.

Some grains are showing an appearance giving the impression that they have been divided into smaller sub-grains. Also signs of grain boundary migration are present, mostly as bulging but also as nucleation.

3.1.4 Thin section 512013

This rock contain the following minerals (with estimated amounts); quartz (40 %), plagioclase (20 %), K-feldspar (25 %), biotite (10 %), chlorite (4 %) and muscovite (1 %). The only observed accessory mineral is zircon (Figure 2).

The rock is homogenous with medium grain size, with the exception of a K-feldspar megacryst in the upper right corner of the thin section Some myrmekite is present. Biotite is commonly showing altered appearance and is often partly or entirely replaces by chlorite. Plagioclase is commonly showing altered appearance and in some cases muscovite is present as inclusion within the grains.

Zircon is associated with K-feldspar, plagioclase, chlorite and quartz to an equal extent. A total of eight zircon grains were observed.

Signs of grain boundary migration are present throughout the thin section, mostly as bulging but also as nucleation. Most quartz, plagioclase and K-feldspar grains are deformed.

3.1.5 Thin section 512028

This rocks has the following mineralogy; quartz (35 %), K-feldspar (35 %), plagioclase (25 %), biotite (<5 %), muscovite (<5 %), garnet (<5 %). Zircon occurs as an accessory mineral (Figure 2).

The rock shows mainly medium grain size, but the grain size is inhomogeneous and quartz, plagioclase and k-feldspar occur as larger grains. Plagioclase and k-feldspar grains abundantly show altered appearance, though some grains are less affected or even unaffected. Small inclusions of myrmekite are present within plagioclase and K-feldspar. The garnet in this rock only occurs as larger grains, which are abundantly fractured. These fractures are filled with biotite and biotite is almost only occurring in association with garnet.

Zircon is associated with quartz, K-feldspar and plagioclase (in order of decreasing frequency). Two of the zircon grains observed in association with K-feldspar also are in contact with quartz.

Signs of grain boundary migration are present, mostly in the form of bulging but also as nucleation. A few possible pseudomorphs of garnet are present.

3.1.6 Thin section 512075

This rock has the following mineral composition; quartz (50 %), plagioclase (25 %), K-feldspar (15 %), biotite (5 %), muscovite (4 %) and garnet (1 %). Zircon is present as an accessory mineral (Figure 2).

The rock shows inhomogeneous grain size, ranging from fine grained to medium grained. Biotite and muscovite only occur as fine grains however. Plagioclase is commonly showing an altered appearance and muscovite is only present in this altered plagioclase. In addition, biotite and k-feldspar is commonly showing altered appearance. The garnet in this rock is almost entirely replaced by plagioclase and biotite.

Zircon is associated with biotite, quartz and plagioclase (in order of decreasing frequency).

Pseudomorphs of garnet are present in the rock, in same cases with small remnant garnet grains present. Grain boundary migration occurs mostly as bulging but also as nucleation. Dislocation migration has been observed in some grains. Some of the plagioclase grains show metamorphic twinning. Quartz is concentrated to band-, vein- or blob-like structures .

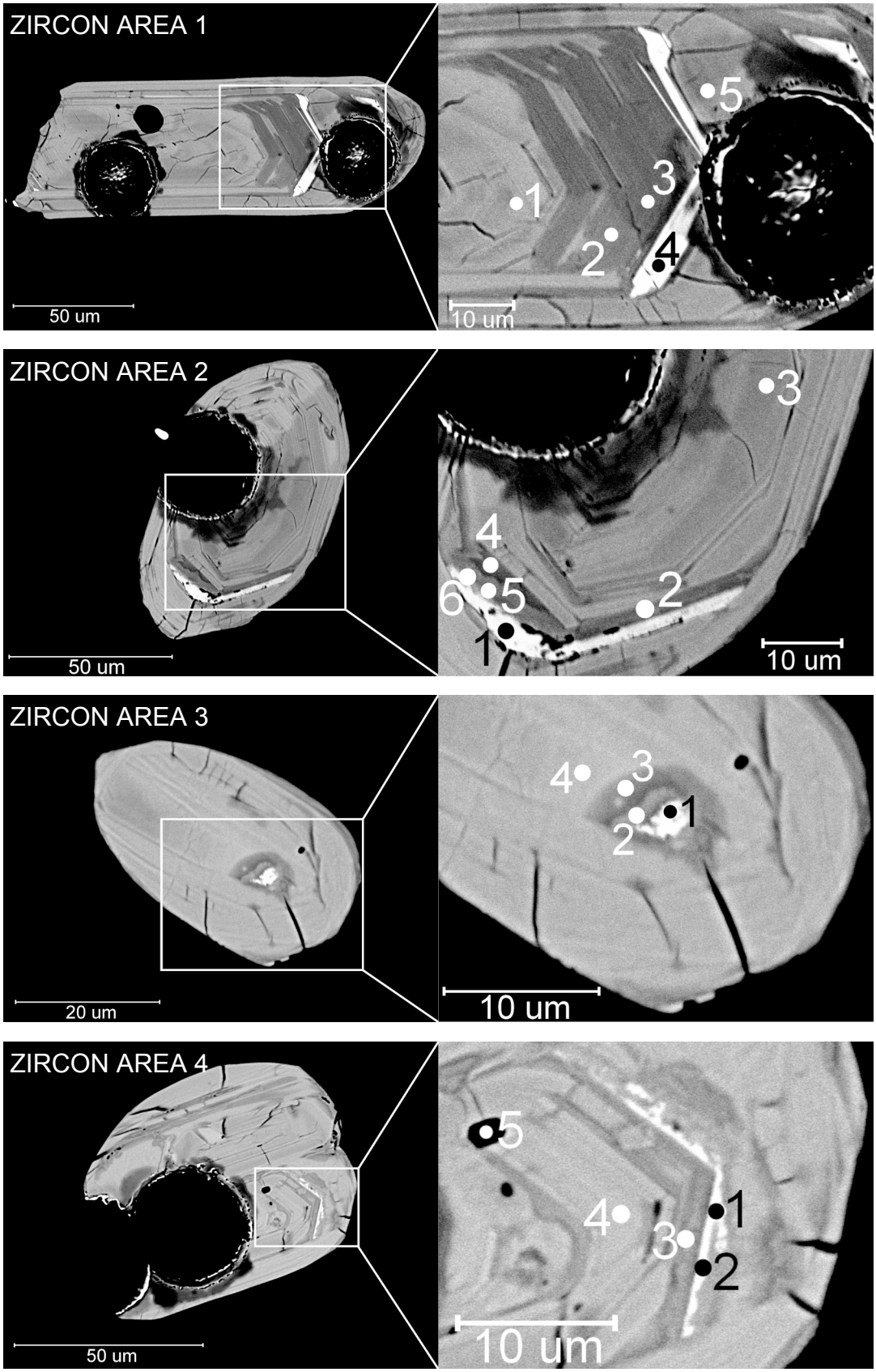

Figure 3: BSE-images of zircon areas 1-4 (from top to bottom) for zircon mount for sample 510155. Zircon appears as grey, baddeleyite as white and inclusions as black. Note that the black circular spots are LA-ICPMS-pits from U-Pb-dating. To the right, enlargements with spots for EDS-analyses are shown. Numbers are listed in Appendix 3.

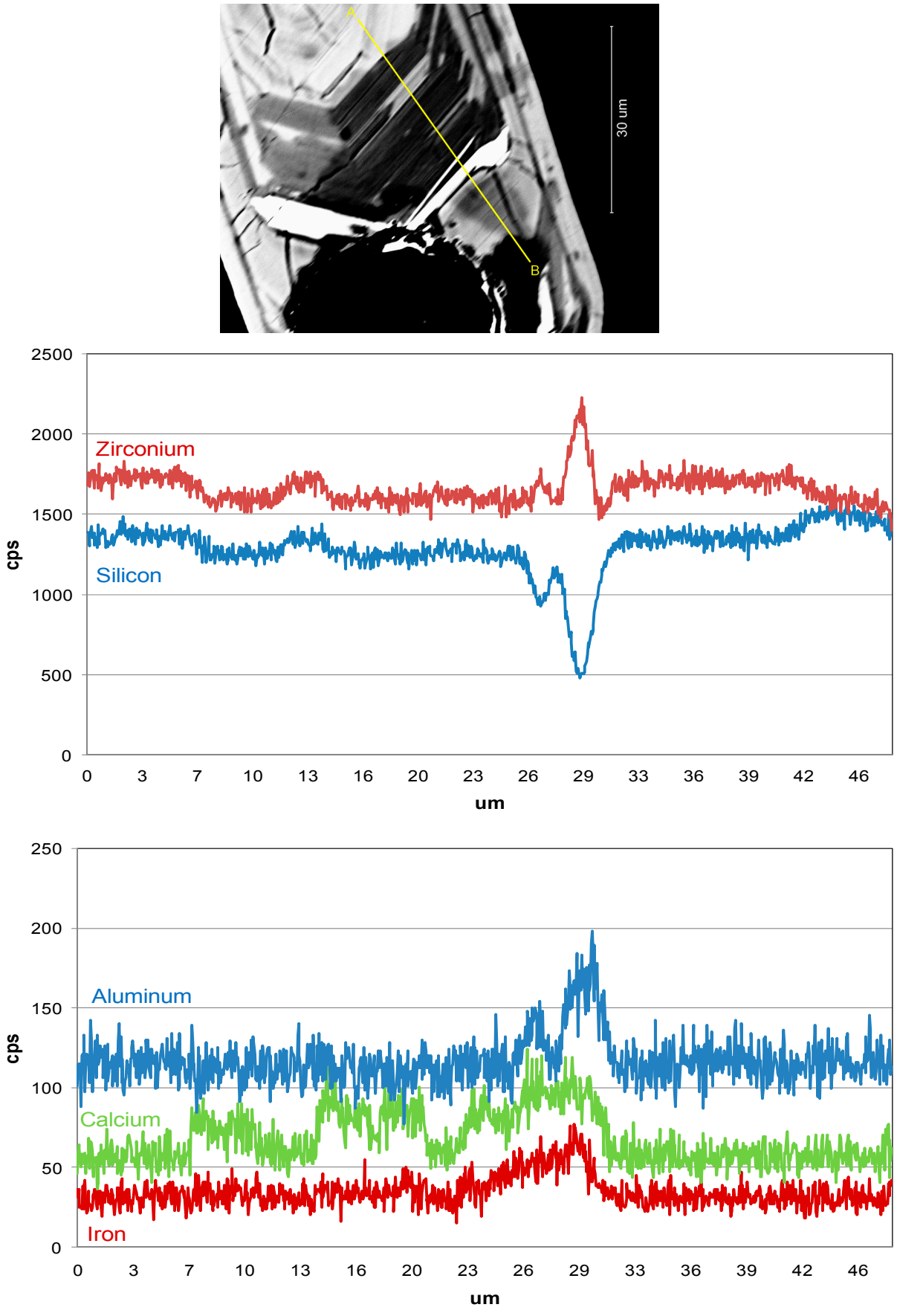

Figure 4: Line scan data for zircon area 1 (zircon mount 510155). The peaks for aluminium, calcium and iron within the baddeleyite domain are noteworthy.

3.2 SEM-EDS

3.2.1 Zircon mount 510155

3.2.1.1 Zircon area 1

As seen in the BSE-image (Figure 3), the centre is magmatically zoned. Although, in the middle-top part of the centre, a large inclusion is present. Towards the larger white baddeleyite domain, the zircon becomes darker. EDS-analyses of these darker domains show the presence of a number of non-stoichiometric elements, such as Ca, Fe and Hf.

Baddeleyite seems to make up one or several parts of the zircon grain's zoning. Further EDS-analyses show that the baddeleyite is impure; it is not entirely Si-free, and contains minor amounts of Al, Ca, Fe, Hf and U. Baddeleyite domains are present as discrete bands in the lower left tip of the grain (Figure 1), as well as a larger domain in the right part of the grain.
Outside the large baddeleyite zone, in a similar fashion as for the core, BSE-imaging shows a magmatically zoned zircon where EDS-analyses show no detectable non-stoichiometric elements. Notable is the presence of several fractures halting at the outer edge of the Bd.

A line scan was made on this zircon area (Figure 4).

3.2.1.2 Zircon area 2

This zircon has a magmatically zoned core with a few fractures present (Figure 3). Also, EDS-analyses of the core show no anomalous elements, i.e. only Si and Zr. In contrast to the core, the part of the zircon closest to the baddeleyite domain show darker appearance during BSE-imaging. These darker domains contain minor concentrations of non-stoichiometric elements, where Na, Al, Ca, Ti, Fe, Nd and Hf were detected during EDS-analyses.

Si is detected within the baddeleyite, although it is significantly lower in contrast to the surrounding zircon. Further, minor amounts of Al, Ca, Ti, Fe, Hf and U are detected and confirm that this is not perfectly pure baddeleyite. Texturally the baddeleyite seemingly occupies one or several of the zircon's growth zones.

Outside the baddeleyite zircon similar to the core is present. Numerous fractures are present, which originate from the outer edge of the zircon and that halt at the outer boundary of the baddeleyite.

3.2.1.3 Zircon area 3

In this zircon no distinct core is observed, although a faint growth zonation is present (Figure 3). EDS-analyses show minor concentrations of non-stoichiometric elements; such as Ca, Fe, Hf and U in the centre of the zircon grain. (Sub)radiating fractures are abundant and seemingly halting at an imaginary ellipsoid shape within the zircon.

Darker zircon surrounds the small baddeleyite domain; which correlates with the presence of non-stoichiometric Na in the darkest rim and Cl, Ca, Fe and Hf in the slightly lighter rim. The largest fracture, originating from the outer boundary of the zircon, halts at the outer boundary of these rims. Noteworthy is that these darker domains, otherwise rather rounded and constant in width around the baddeleyite, apparently stretch out to connect with the large fracture.

The baddeleyite domain is impure, where EDS-analyses detect non-stoichiometric Al, Si, Ca, Fe, Hf and U. The position of the Bd-domain within the zircon appears to be non-related to the inner structure of the zircon.

3.2.1.4 Zircon area 4

In general this is a structurally and texturally complex zircon; with both domains showing magmatic zoning and domains not showing zoning, as well as numerous inclusions, present (Figure 3). One of the inclusions consists of Mg, Al, Si, K, Fe and Zr.

Several darker domains are present in the BSE-images (i.e. domains with lower density), associated with both zoned and non-zoned parts of the zircon as well as the baddeleyite. The darker domain associated with the baddeleyite is seemingly part of the magmatic zoning. EDS-analyses of this darker domain show presence of non-stoichiometric Cl, Ca and Fe.

The baddeleyite domain is part of a non-zoned domain of the zircon, or at least the zoning of the zircon halts with the transition to baddeleyite. It is chemically impure and show non-stoichiometric Al, Si, Ca, Ti, Fe, Hf and U.

3.2.2 Zircon mount 512028

3.2.2.1 Zircon area 1

This ~200 µm long zircon has a core with magmatic zoning, though in both zircon area 1a and 1b some smaller spots as well as few tiny inclusions are present. In addition several fractures can be seen in the core, especially in the part of the zircon presented as zircon area 1b. Outside the core a rather uniform layer, not far from completely encapsulating the core, of darker appearing zircon is observed. EDS-analyses of this layer show no sign of anomalous elements. This layer is also the inner boundary between the zircon and the baddeleyite domains (Figure 4).

The baddeleyite domains occur in both ends of this zircon (zircon area 1a and 1b). They are following the magmatic growth zoning. Further, they are impure and their respective Si-content does not entirely drop to nil. In ZA 1a EDS-analyses show non-stoichiometric Al, Cl, Ca and Fe; whilst in ZA 1b the anomalous elements are limited to Al, Ca and Fe. The baddeleyite domain in ZA 1b is interlayered by a very dark zircon in the outer part of the domain. This dark zircon is non-stoichiometric and contains Na, Al, Cl, Ca and Fe.

Outside the baddeleyite domain (in both ends) the zircon shows growth zoning and no sign of anomalous elements. In the upper end the zircon has faint zoning and towards its outer boundary numerous fractures and inclusions appear. Notable is small domains of a slightly darker zircon seemingly growing from the fracture (and related inclusions) and replacing the original structure. In contrast the outermost part of the

lower end of the zircon show more distinct zoning but also more extensive fracturing and a slightly darker appearance. Mostly the fractures halt at the outer boundary of the baddeleyite, but one of them crosscuts the outer baddeleyite layer at two locations.

3.2.2.2 Zircon area 2

This zircon has no distinct core with only the areas below and to the left of the baddeleyite show some sort of zoning. In this area a large inclusion associated with numerous fractures is present. The areas above and to the right of the baddeleyite are divided into two respectively homogenous domains where the larger domain is slightly darker than the smaller domain. EDS-analyses show no non-stoichiometric elements in the zircon. The inclusion consists of Al, Si, Ca, Fe and Zr (Figure 4).

The outer boundary of the baddeleyite domain is roughly following the zoning system of the zircon in the bottom-right and bottom-left parts. The upper parts of the domain do not show such pattern. It is not Si-free and contains minor amounts of Al, Ti and Fe. Numerous fractures, originating from the outer boundary of the zircon grain, penetrate all the way into the baddeleyite domain.

3.2.2.3 Zircon area 3

This zircon grain does not show a magmatic zoned core. In the outer parts of the grain a faint zoning can be observed. It becomes successively lighter in three distinct levels towards the centre. Numerous fractures are penetrating the grain from its outer boundary, all the way into the centre. EDS-analyses show no anomalous zircon compositions in the outer part of the grain (Figure 5).

The centre is in general occupied by a large baddeleyite domain, a smaller and entirely black inclusion as well as a distinctly darker zircon (in comparison with the zircon outside the centre). The darker zircon occupies the outermost-bottom part of the centre. It shows no zoning. EDS-analyses show non-stoichiometric Na, Cl, Ca and Fe. The inclusion is situated in the outermost-right part of the centre. It is associated with an accentuated fracture system. EDS-analyses show that it consists of Al, Si, Ca, Fe and Zr. In the middle and upper parts of the centre the baddeleyite domain is observed. Within the domain more or less elongated and sub parallel inclusions are present (striking at ~315° from the horizontal plane). EDS-analyses of the baddeleyite show that it is not Si-free and contain minor concentrations of Al, Si, Cl, Ca, Mn, Fe and U.

3.2.2.4 Zircon area 4

This zircon grain consists of two distinctly different areas. The grain has a rim of magmatically zoned zircon, and is abundantly fractured. These fractures are seemingly halting at the boundary to the centre of the grain. EDS-analyses show no anomalous non-stoichiometric composition for this area (Figure 5).

In the centre of the grain, two components are present; a seemingly homogeneous dark zircon and an intricate baddeleyite complex. The baddeleyite occurs in bands, interlayered by dark zircon. Its structure appears rather similar to the one of a magmatic zoned zircon. Through EDS-analyses it has been determined that the baddeleyite is not entirely Si-free and contains minor amounts of Al, Ca and Fe. In the middle parts of the centre, non-zoning like baddeleyite is present. Based on BSE-images it is more impure (i.e. darker appearance) than the one represented as layers.

EDS-analyses of the darker zircon show non-stoichiometric Na, Ca and Fe. In the middle to upper left parts, the centre seems overprinted by brighter zircon. Based on BSE-images the composition of this zircon is similar to the one in the rim, although it does not show any zoning.

3.2.2.5 Zircon area 5

The BSE-image of this zircon is dark, but a magmatic zoning is observed, which also can be seen in the CL-image. Baddeleyite is present as bands, which are part of the grain's zoning system. The outer parts of the grain are somewhat fractured (Figure 5).

3.2.2.6 Zircon area 6

This zircon grain shows magmatic zoning, particularly in the CL-image. The baddeleyite occurs in bands, concordantly with the internal structure of the grain. The zircon present outside the baddeleyite is abundantly fractured and these fractures are seemingly halting at the outer boundary of the baddeleyite domain (Figure 5).

3.2.2.7 Zircon area 7

The centre of this zircon grain consists of non-zoned zircon, baddeleyite and an unidentified inclusion. On both sides of the baddeleyite, the zircon is slightly darker compared to the rest of the grain. Outside the centre, the zircon shows magmatic zoning. There are numerous inclusions, that originate from the outer margin of the grain and that are halting at or near the boundary to the centre (Figure 6).

3.2.2.8 Zircon area 8

This is a complex zircon grain showing many convolute features. In the left side centre of the grain, a non-zoned zircon and a black inclusion is surrounded by a zircon showing magmatic zoning. It is notable that this zoning is discordant to the zoning present in the rest of the grain. To the left of the non-zoned zircon mentioned above, an amorphous baddeleyite domain is present (Figure 6).

The right side of the centre show very few distinct structures. This area is mostly occupied by an unzoned and slightly darker zircon (compared to the one outside this area). Numerous black inclusions are present, sometimes in contact with baddeleyite. In addition, some of the white lumps are not baddeleyite. EDS-analyses of some of them show that they are slightly

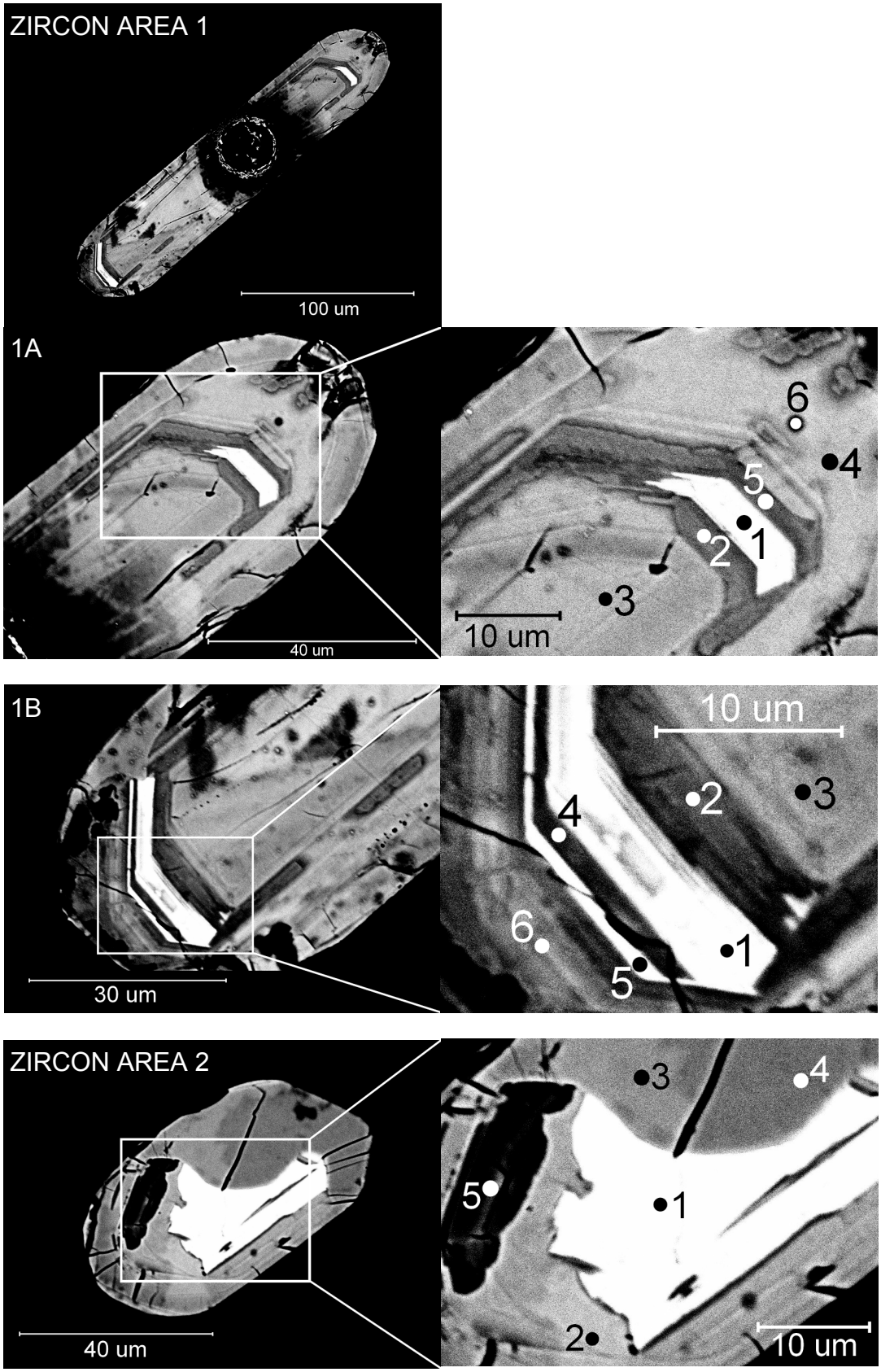

Figure 4: BSE-images of zircon areas 1 and 2 (from top to bottom) for zircon mount for sample 512028. Zircon appears as grey, baddeleyite as white and inclusions as black. Note that the black circular spot is a LA-ICPMS-pit from U-Pb-dating. To the right, enlargements with spots for EDS-analyses are shown. Numbers are listed in Appendix 3.

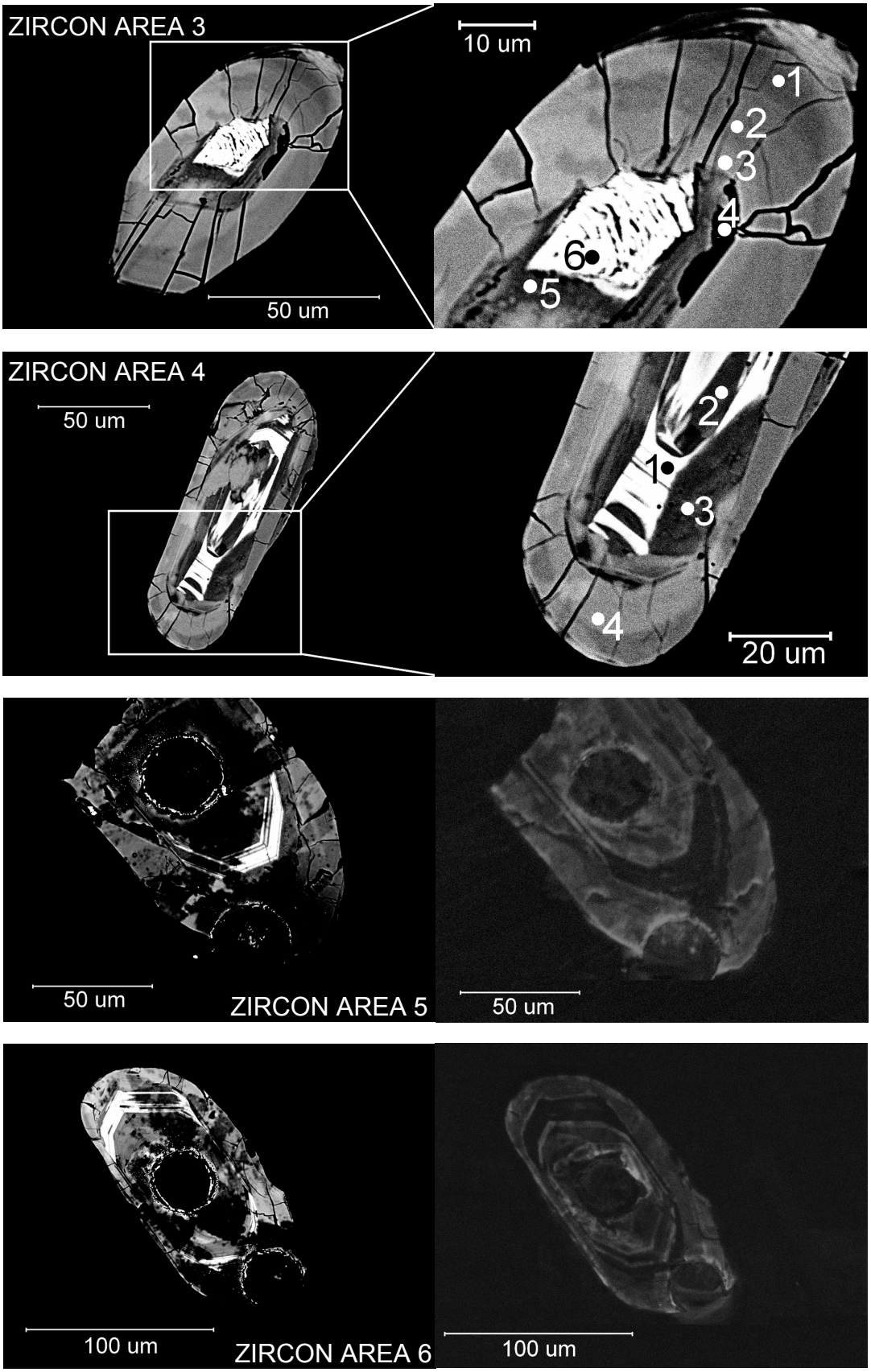

Figure 5: BSE-images of zircon areas 3-6 (from top to bottom) for zircon mount for sample 512028. Zircon appears as grey, baddeleyite as white and inclusions as black. To the right, enlargements with spots for EDS-analyses are shown (zircon area 3 and 4) and CL-images are presented (zircon area 5 and 6). Numbers are listed in Appendix 3.

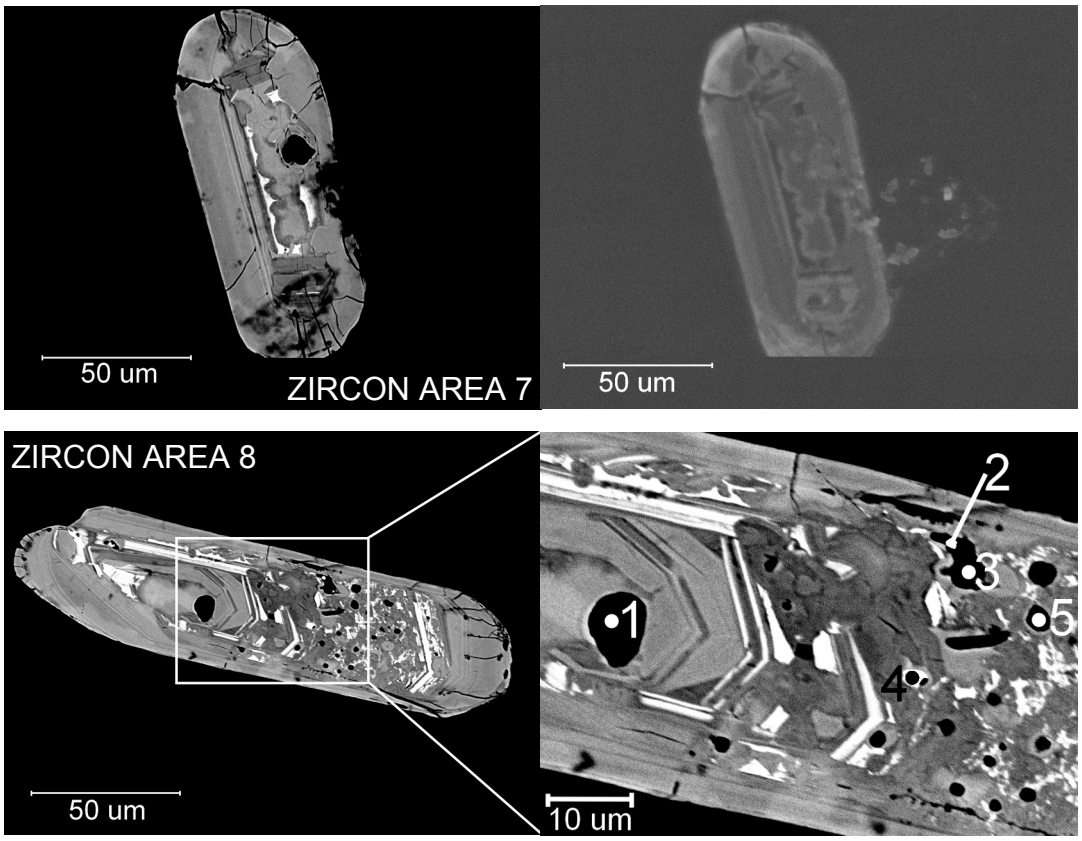

Figure 6: BSE-images of zircon areas 7 and 8 (from top to bottom) for zircon mount for sample 512028. Zircon appears as grey, baddeleyite as white and inclusions as black. To the right, enlargements with spots for EDS-analyses are shown (zircon area 8) and a CL-image is presented (zircon area 8). Numbers are listed in Appendix 3.

impure heavy metal oxides; containing Pb, Th and U. In this area, baddeleyite occurs both as bands (following the general zoning structure of the grain) and as lumps. EDS-analyses show that the black inclusions in the centre of this grain consist of slightly impure quartz with minor amounts of Na, Al, Ca, K and Zr.

The layer outside the centre is occupied by a magmatically zoned zircon and some baddeleyite. The baddeleyite is mostly following the zoning structure of the zircon. At the right short side of the zircon a few inclusion associated with fractures are present. Numerous fractures, halting at the boundary to the centre, are present in this layer.

3.2.3 Thin section 468720

3.2.3.1 Zircon area 1

This zircon grain is surrounded by quartz. The whole grain is abundantly fractured, which are mostly parallel. The core shows magmatic zonation. In the upper part of the grain, this zonation is cut by the outer zircon rim. The left part of the core as well as the right part of the rim has darker appearance in BSE-images. EDS-analyses of this darker zircon show that it contains non-stoichiometric Al and Fe (Figure 7).

Baddeleyite occur both as bands and as patchy irregular structures. It also occurs in both the core and the rim. Baddeleyite is present in the top right part of the grain along the outer margin. There it is in direct contact with the surrounding quartz grain. EDS-analyses of the baddeleyite in this grain show that it not Si-free. In addition, minor amounts of Al are detected in the core and Al and Fe in the rim.

The zircon grain is situated along a major fracture system in the surrounding quartz grain.

3.2.3.2 Zircon area 2

This zircon grain (Figure 7) is surrounded by quartz, but at the bottom only a few microns from plagioclase. It shows magmatic zoning. In the centre of the grain, baddeleyite occur as a band, concordant with the primary zonation of the zircon. Outside this band two fractures originating from the rim halt at the outer boundary of the baddeleyite. EDS-analyses of this zircon show no anomalous compositions. In the rim, baddeleyite occur as a band semi-concordant with the zonation. The appearance is more irregular; however the band is not uniform. In the bottom of the original grain (in the thin section most of the bottom part of the grain is gone) isolated baddeleyite blobs are present. EDS-analyses of the baddeleyite show that it contains small amounts of Si and minor amounts of Al, Fe and Ca. Outside the outer baddeleyite domain a darker (in BSE-images) zircon is present. EDS-analyses of this zircon show non-stoichiometric Al, Fe and Ca. This

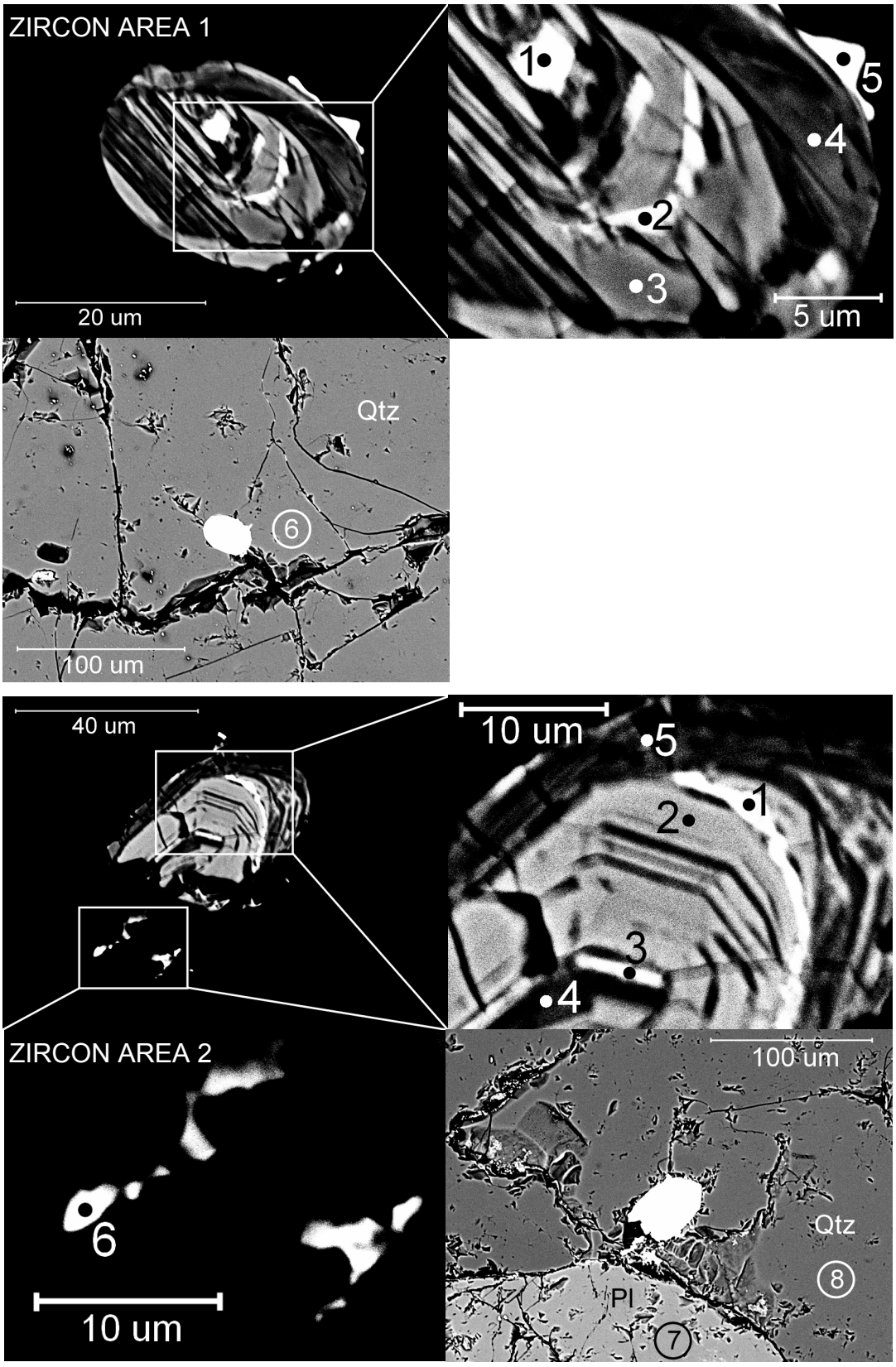

Figure 7: BSE-images of zircon areas 1 and 2 (from top to bottom) for thin section 468720, as well as corresponding surroundings. Zircon appears as grey, baddeleyite as white and inclusions as black (surroundings excluded, where zircon appears as white and other surrounding minerals as grey-black). Zircon area 1: mineral 6 is quartz. Zircon area 2: mineral 7 is plagioclase and 8 is quartz. Enlargements and spots for EDS-analyses are shown and numbers are listed in Appendix 3.

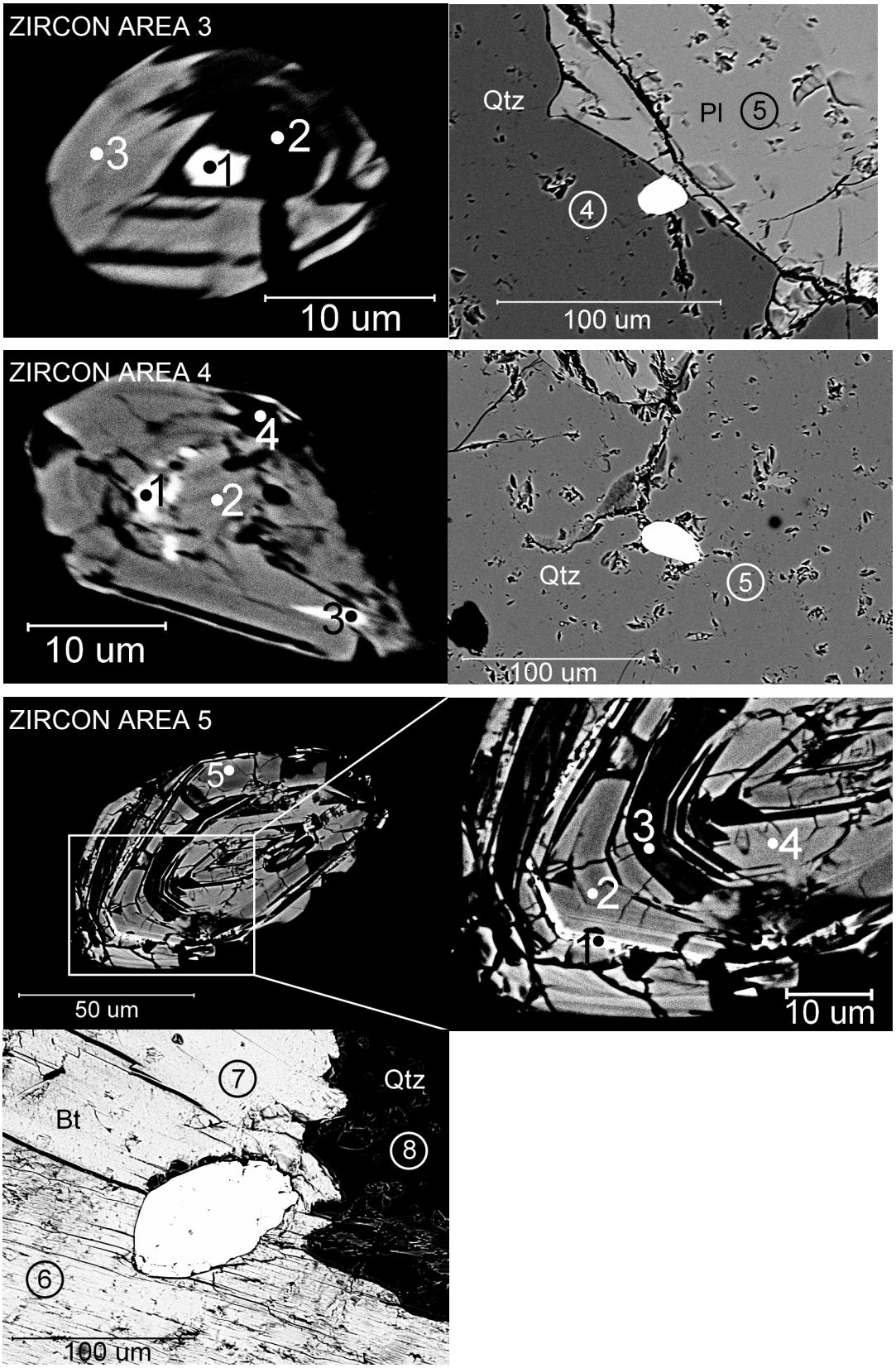

Figure 8: BSE-images of zircon areas 3-5 (from top to bottom) for thin section for sample 468720, as well as corresponding surroundings. Zircon appears as grey, baddeleyite as white and inclusions as black (surroundings excluded, where zircon appears as white and other surrounding minerals as gray-black). Zircon area 3: mineral 4 is quartz and 5 is plagioclase. Zircon area 4: mineral 5 is quartz. Zircon area 5: mineral 6 and 7 is biotite, 8 is quartz. Enlargements with spots for EDS-analyses are shown and numbers are listed in Appendix 3.

zircon grain is associated with an extensive fracture system in the surrounding quartz grain.

3.2.3.3 Zircon area 3

This zircon grain (Figure 8) is primarily surrounded by quartz, but it is also in contact with plagioclase. It shows no distinct zonation. A major part of the grain is showing nearly to totally black appearance in BSE-images. EDS-analyses of these black areas show that they consist of Zr, Fe, Si, Al and Ca (in order of concentration by stoichiometry, from high to low). In the centre of the grain a irregular patchy baddeleyite domain is present. It is surrounded by black zircon. This baddeleyite domain is not Si-free. Further, the detection of minor amounts of Fe, Al and Ti illustrates that it is impure. The adjacent grains are fractured and the zircon grain is associated with a major fracture in the quartz grain.

3.2.3.4 Zircon area 4

This zircon grain is surrounded by quartz. The zircon shows magmatic zoning. The whole grain is fractured and numerous inclusions (black spots), often associated with fractures, are present. SEM-analyses of the zircon show no anomalous compositions. Baddeleyite occurs as several patchy irregular domains, seemingly with no connection to the primary zonation of the zircon. These domains are associated with fractures in the grain. SEM-analyses of the baddeleyite show that it is not Si-free and contains minor amounts of Al and Fe. The surrounding quartz grain is fractured and the zircon grain is situated along one of these fractures (Figure 8).

3.2.3.5 Zircon area 5

This zircon grain is surrounded by biotite (Figure 8). The grain is magmatically zoned. Consistent throughout the grain is the interlayered texture, where two types of zircon are present. The grey (in BSE) zircon shows no anomalous elements. In contrast, the black (in BSE) zircon is impure, which is indicated by lower silica content and the detection of minor amounts of Fe, Al and Ca. Further, the whole grain is abundantly fractured. Baddeleyite occurs as a jumble of small patchy blob-like structures, in the bottom-left part of the grain. The left-most part of the baddeleyite domain is more regular and band-like. The baddeleyite is ostensibly occurring concordant with the primary zonation of the zircon. EDS-analyses of the baddeleyite show that it is not Si-free. Furthermore, minor amounts of Fe, Al and Ca are detected. The surrounding grain is abundantly fractured along the cleavage planes. Quartz is present adjacent to the biotite.

3.2.4 Thin section 510155

3.2.4.1 Zircon area 1

Firstly, this is the least convincing example of in situ Bd-bearing zircon in this sample (Figure 9). The zircon grain is situated within plagioclase. It shows distinct magmatic zoning, although in the far left and right part the zoning is less prominent. Some domains show darker parts situated in the core as well as the outer parts. Several inclusions are present. Numerous fractures are present, seemingly concentrated to a layer within the zone system and halting at the core. Baddeleyite occur as part of the primary magmatic zone structure and it is also associated with a dark domain of the zircon. EDS-analyses of the baddeleyite show that it is not totally Si-free and that it contains minor amounts of Al and Ca. Several fractures within the host grain are originating from the zircon.

3.2.4.2 Zircon area 2

The zircon is mainly situated in plagioclase, but also has boundaries to both biotite and apatite. The centre of this zircon shows no magmatic zoning; on the contrary it largely consists of a darker domain as well as some black spots. Outside the centre there is a thin layer where the zircon is faintly zoned. Further away from the centre the zircon becomes darker and baddeleyite occur (Figure 9).

The baddeleyite domain appears to be part of the zircon's zoning system and occurs as a minor band. Through EDS-analyses the impure and not entirely Si-free baddeleyite has been determined to contain minor amounts of Al, Ca, Ti, Fe and Hf.

At the outer boundary of the baddeleyite, the zircon shows magmatic zoning in similar manner as the layer outside the centre. In contrast, this layer is pierced by several fractures originating from the outer boundary of the zircon and halting at or near the baddeleyite.

The surrounding contains abundant fractures and the adjacent plagioclase grain is the most heavily fractured. The zircon is seemingly situated as a fracture node.

3.2.4.3 Zircon area 3

This zircon grain is surrounded by biotite. In this zircon, the core is magmatically zoned and shows no sign of recrystallisation, inclusions or metamictisation; with exception for a small darker spot in the upper part of the core associated with the large fracture almost crosscutting the whole zircon. Outside the core, a distinct darker layer is present, in the upper part of the zircon marking the transition to baddeleyite (Figure 10).

The baddeleyite seem to follow the zircon's zoning pattern. The baddeleyite is not completely Si-free and contains minor amounts of Al, Ca, Sc, Ti, Fe, Hf and U. In the upper part of the zircon, outside the baddeleyite, the zircon shows similar behaviour to that in the darker layer whilst the left part of the zircon (where no baddeleyite is present) is zoned and similar to the core.

A fracture in the host grain, continuing into the adjacent apatite grain, halts at the boundary to the zircon. NOTE: the clusters of small white spots in the picture showing the surroundings are dirt being trapped between the thin section and the carbon coating.

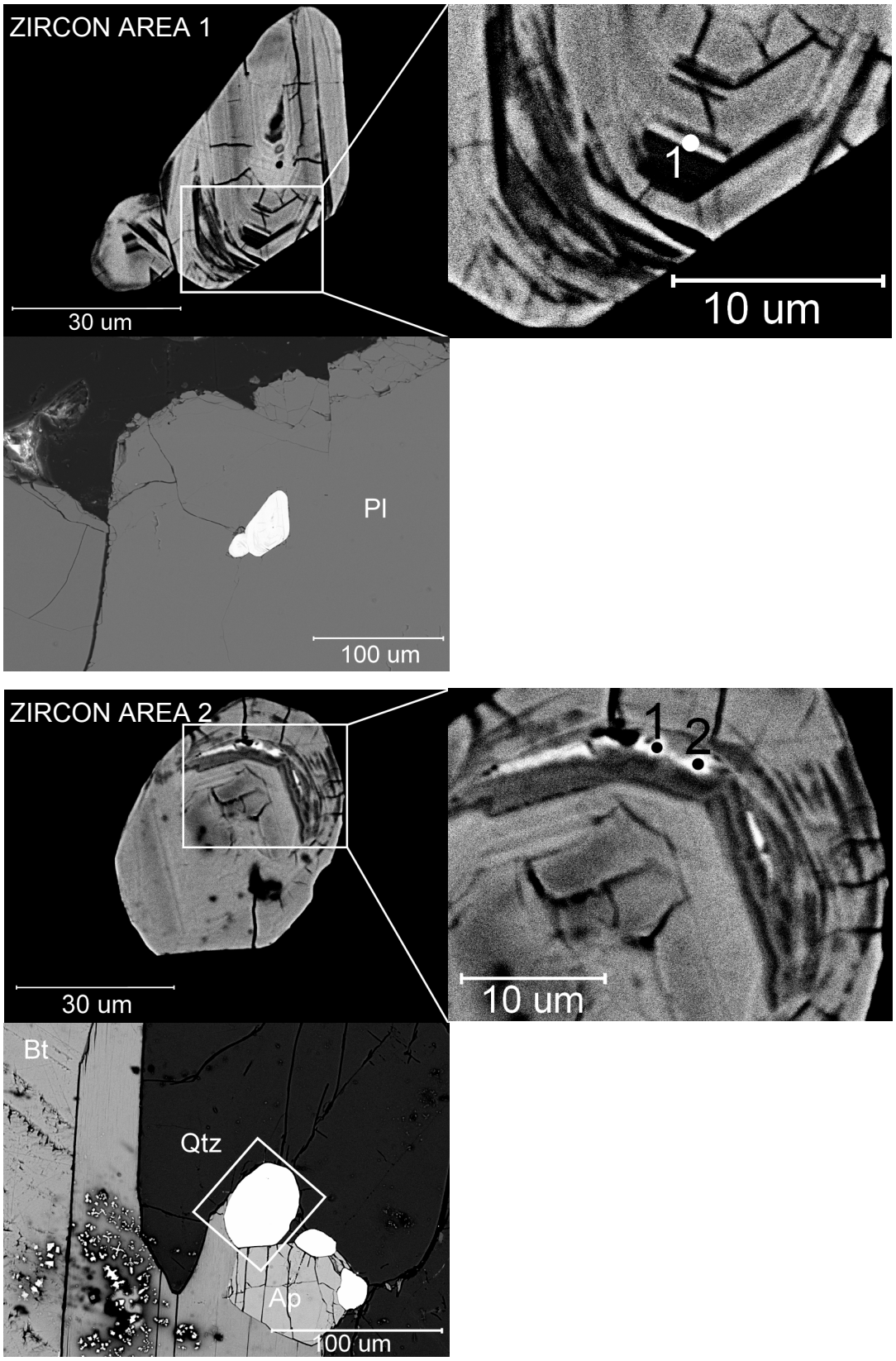

Figure 9: BSE-images of zircon areas 1 and 2 (from top to bottom) for thin section for sample 510155, as well as corresponding surroundings. Zircon appears as grey, baddeleyite as white and inclusions as black (surroundings excluded, where zircon appears as white and other surrounding minerals as grey-black). Enlargements with spots for EDS-analyses are shown and numbers are listed in Appendix 3. Zircon area 2: the clusters of small white spots are dirt being trapped between the thin section and the carbon coating (lowermost picture).

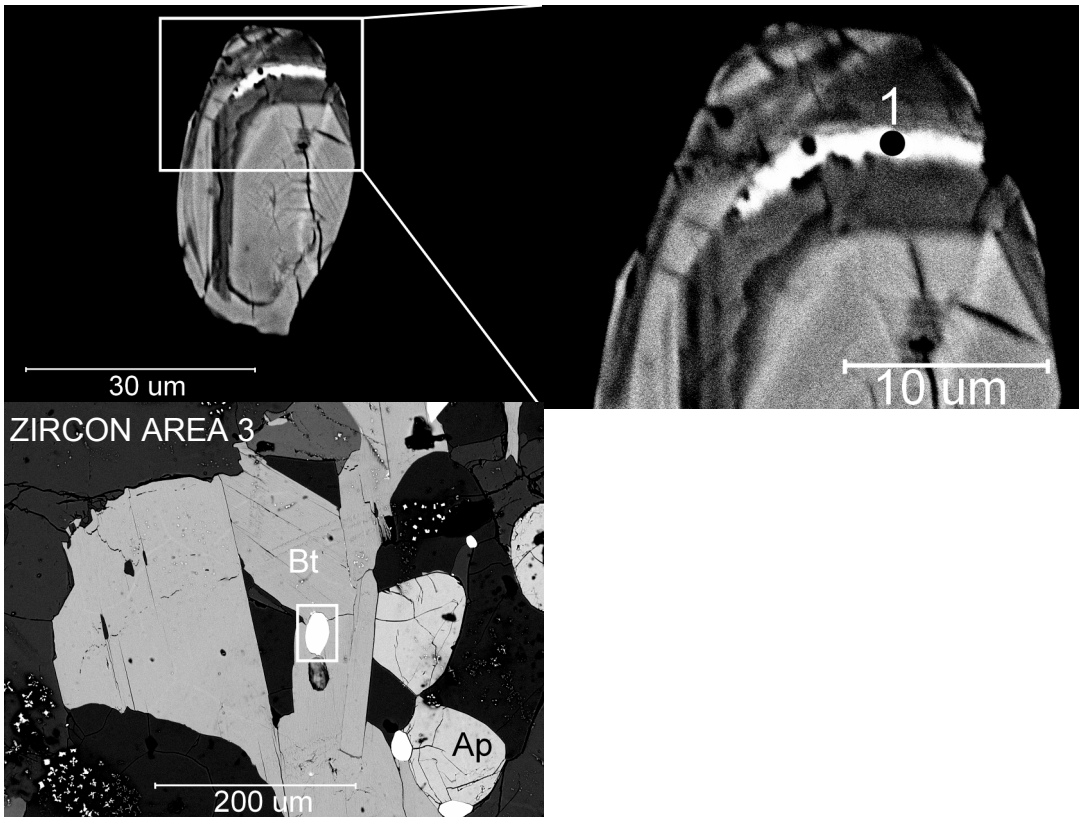

Figure 10: BSE-images of zircon area 3 for thin section for sample 468720, as well as corresponding surrounding. Zircon appears as grey, baddeleyite as white and inclusions as black (surroundings excluded, where zircon appears as white and other surrounding minerals as grey-black). Enlargements are shown with spots for EDS-analyses and numbers are listed in Appendix 3.

3.2.5 Thin section 512028

3.2.5.1 Zircon area 1

This zircon grain is surrounded by quartz. The core shows a mottled texture, and baddeleyite occurs as arbitrarily shaped structures, seemingly positioned totally at random. Further, a few less dense (totally black in BSE-images) inclusions are present in the core. EDS-analyses of one of these Bd-domains show that it is impure. Further, it is not Si-free and shows minor amounts of Al, Ca, Ti, Fe and U (Figure 11)

The boundary between the core and the rim is distinct and the rim shows a faint zoning. Baddeleyite domains mainly occur along this boundary. A few baddeleyite domains are present outside the core-rim boundary and here they seem to follow the zoning of the zircon. Numerous fractures and inclusions are present in the rim. EDS-analyses of one of the core-rim-domains show that it is impure, contains small amounts of Si as well as minor amounts of Al, Ti, Fe, and U.

The host quartz grain show abundant fractures originating from the zircon. Other grains adjacent to the quartz grain are K-feldspar and plagioclase. The Kfs grain is heavily fractured and along these fractures an unidentified mineral is present.

3.2.5.2 Zircon area 2

This zircon grain is surrounded by quartz (Figure 11). It shows a distinct magmatic zoning throughout the whole grain. In the outer parts of the grain a few inclusions and fractures are present. The large white Bd-domain in the left part of the grain occurs as a banded and as part of the zoning system. In addition, a less distinct Bd-band is present in the right part of the grain. EDS-analyses show that the baddeleyite is impure. It is not Si-free and contains minor amounts of Al, Ca, Fe and U. Inside the baddeleyite band, the zircon show slightly darker appearance in comparison with the rest of the grain. This darker zircon, also extends a few microns outside the baddeleyite band.

The host grain is abundantly fractured where numerous fractures are originating from the zircon grain.

3.2.6 Thin section 512075

3.2.6.1 Zircon area 1

This zircon grain is surrounded by quartz. It shows magmatic zonation and is abundantly fractured. Numerous inclusions, often associated with fractures, are present. The centre of the grain shows slightly lighter appearance in BSE compared to the rim. However, SEM-analyses show no compositional difference or anomalous elements (Figure 12).

Baddeleyite occurs in two textural contexts, as

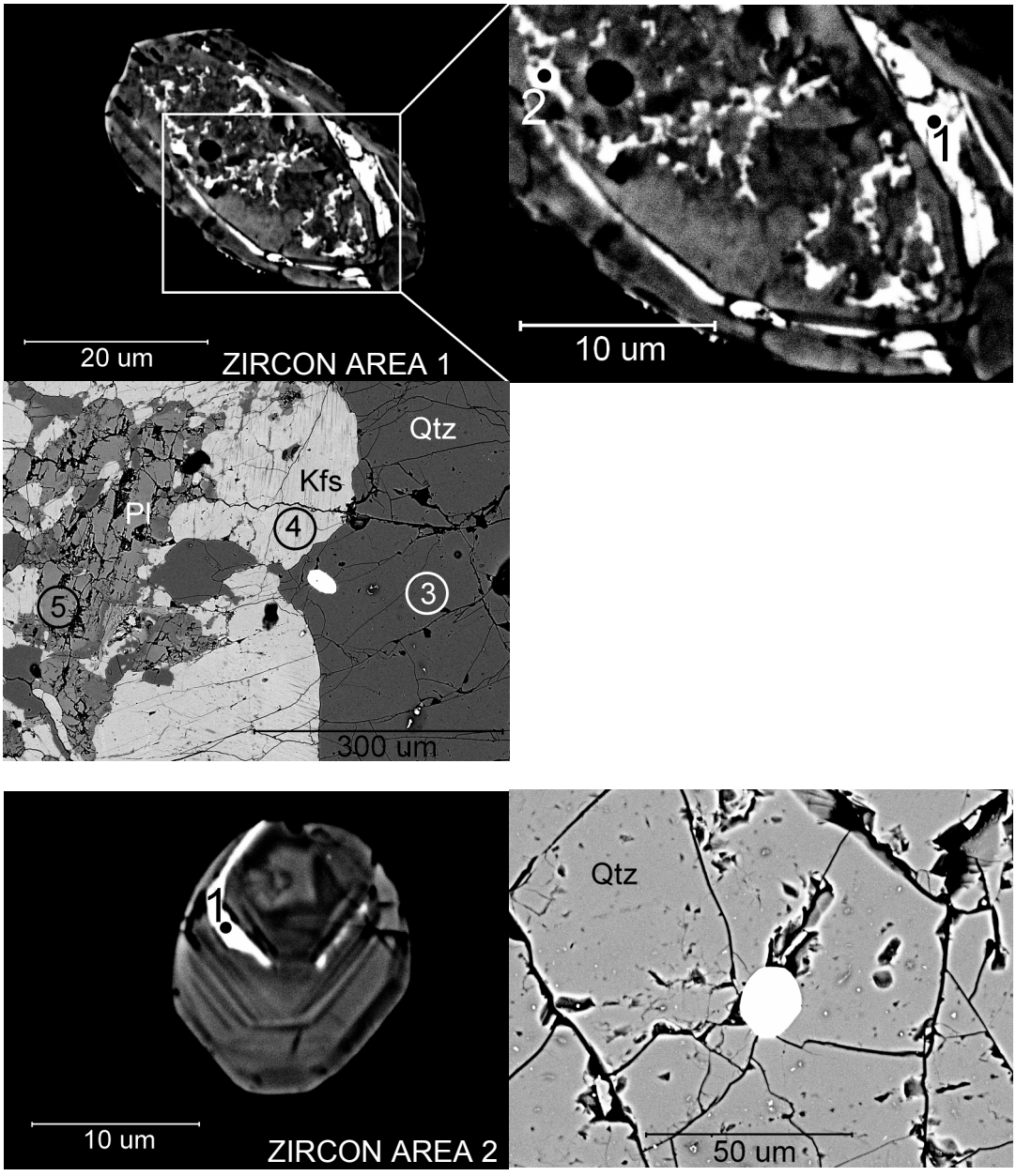

Figure 11: BSE-images of zircon areas 1 and 2 (from top to bottom) for thin section for sample 512028, as well as corresponding surroundings. Zircon appears as grey, baddeleyite as white and inclusions as black (surroundings excluded, where zircon appears as white and other surrounding minerals as grey-black). Zircon area 1: Mineral number 3 is quartz, 4 is k -feldspar and 5 is plagioclase. Enlargements and spots for EDS-analyses are shown and numbers are listed in Appendix 3.

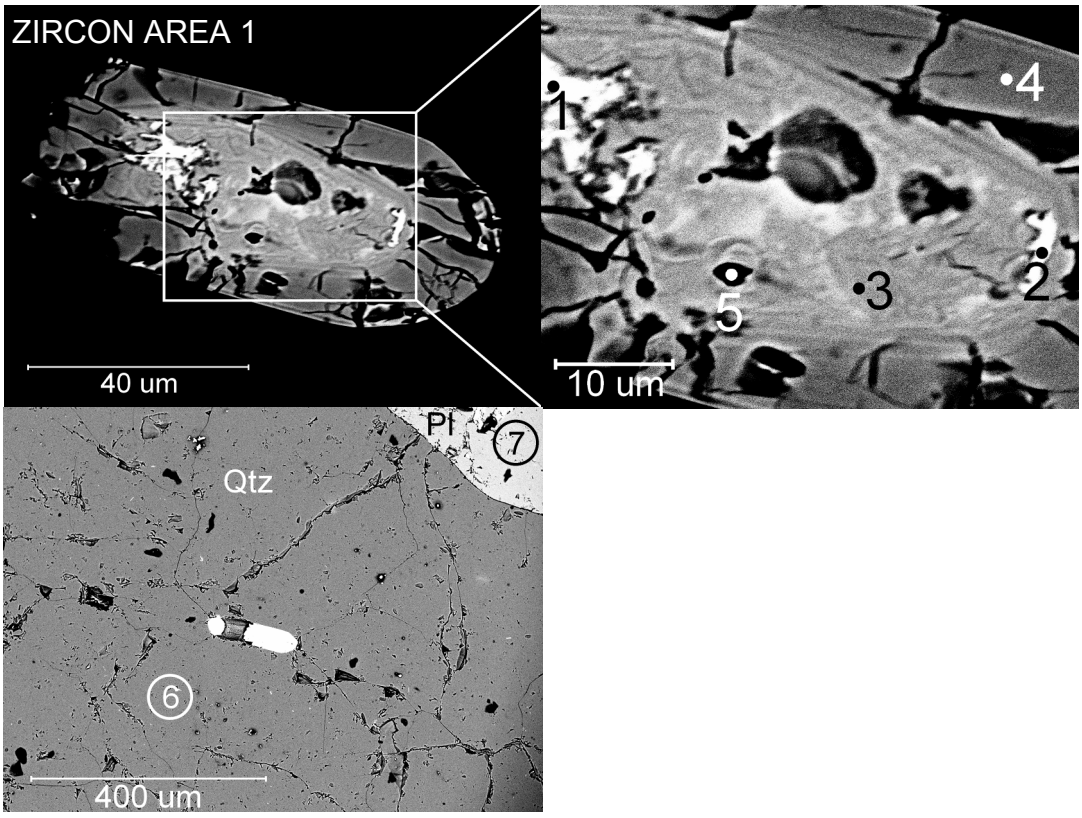

Figure 12: BSE-images of zircon area 1 for thin section for sample 512075, as well as corresponding surroundings. Zircon appears as grey, baddeleyite as white and inclusions as black (surroundings excluded, where zircon appears as white and other surrounding minerals as grey-black). Mineral number 6 is quartz and 7 is plagioclase. Enlargements and spots for EDS-analyses are shown and numbers are listed in Appendix 3.

patchy scattered domains in the outer parts of the brighter zircon. In the left part of the grain, a larger domain occurs. EDS-analyses show that it is not Si-free and contains minor amounts of Al, Ca, Ti, Fe and Hf. In the right part of the grain the domain is smaller. This domain differs from the other one by the detection of U and the lack of Ti and Hf. Both domains are associated with fractures. These fractures originate from the outer edge of the zircon grain and halt at the outer boundaries of the baddeleyite domains.

The surrounding quartz is slightly impure, containing smaller amounts of Al and Th. Fractures are abundant throughout the grain and the right tip of the zircon grain is situated in a fracture triple junction. A plagioclase grain is present adjacent to the quartz grain.

3.3 Geochemistry

Normative calculations (CIPW-norm) were made for four of the samples. It is notable that all of the samples are containing normative corundum (i.e. they are peraluminous).

Further, the zircon saturation temperature was calculated to around 750 °C. Numbers are presented in Appendix 5. All calculations were made with the software Geochemical Data Toolkit (GCDkit) (Janoušek et al. 2006).

4 Discussion

4.1 Zircon occurrence

Zircon is occurring in association with biotite, quartz, plagioclase, K-feldspar and apatite in the rocks studied here. There is no clear link between zircon occurrences and surrounding mineral. However, zircon is most commonly occurring in association with biotite and quartz.

Furthermore, SEM-imaging shows that baddeleyite bearing zircon grains are to great extent surrounded by quartz, which seems to imply steep geochemical gradients as quartz should buffer SiO_2 and keep zircon stable. Only a few of the studied zircon grains are surrounded by or in contact with other minerals (biotite, plagioclase and apatite).

The zircon saturation temperatures calculated (~750 °C) could suggest that zircon has crystallised over a large interval of the formation of the rocks. E.g. in sample 510155 (the NGI granite), zircon grains are present in all mineral phases of the rock and this correlates well with the calculated zircon saturation temperature. It is not possible to link the zircon saturation temperature to the formation of baddeleyite however. A rather large possible error source is the presence of baddeleyite in these rocks, making the apparent zircon concentration higher than the actual.

4.2 SEM-EDS

There are two different textural occurrences of these baddeleyite domains; as bands concordant with the primary zircon zonation, and as patchy irregular blob-like domains. It is possible that these occurrences are derived from different processes. In some cases baddeleyite occur along the outer margin of the zircon grain. It is notable that, in these cases, the baddeleyite is in direct contact with quartz.

The baddeleyite domains are impure. They are not silica-free and minor amounts of trace elements, such as uranium and hafnium, are also detected within the baddeleyite. The most striking observation however, is the detection of aluminium, calcium and iron in the baddeleyite. This is especially well illustrated by the line scan results.

Towards each baddeleyite domain, zircon often becomes darker in BSE. EDS-analyses demonstrate that the darker zircon is impure; containing minor amounts of non-stoichiometric elements, such as calcium, iron, sodium and titanium.

The part of the zircon grain outside the baddeleyite domain is often abundantly fractured. The fractures usually stop at or near the outer boundary of the baddeleyite domain. This pattern correlates especially well for the patchy irregular baddeleyite occurrences.

Possible sources of error for the EDS-analyses are: For a large number of analyses the EDS spot size was larger than the analysed area. Therefore many of the EDS-analyses are composite analyses of several minerals, domains or zones. This could imply detection of elements that are not present in the marked spot. The detection of silica in the baddeleyite could be a disturbance effect from underlying zircon. Since the baddeleyite domains are small (and probably thin), this is rather probable. Yet, the silica amounts are rather similar in all analyses (mean = 0.31, relative standard deviation = 50 %, n = 29).The detection of chlorine in some EDS-analyses could be a disturbance effect from the epoxy in the mount, which contains chlorine. A systematic error is also present throughout the EDS-analyses, making the stoichiometric silica-zirconium ratio become ~0.88:1.12 instead of the presumed 1:1. This makes it impossible to compare the analyses quantitatively. Although it is still possible to make qualitative and relative comparisons, both within grains and between grains.

4.3 Primary or secondary processes?

The baddeleyite occurrence concordant with the primary structure is, as earlier mentioned, well ordered and symmetric. This suggests an origin derived from a primary process (i.e. crystallisation from a magma). This hypothesis is testable as the age of the host rock and host zircon is known in many cases, and a contemporaneous baddeleyite, would support a primary origin. Such detailed geochronology is beyond the scope of this study however.

Patchy and irregular baddeleyite occurrences lack connection to any primary structure. Therefore it is improbable that their origin is of a primary nature. A darker zircon, recognised in EDS-studies by significantly lower silica content and the detection of anomalous elements, e.g. sodium and calcium, is often associated with this type of occurrence. In one of the samples (468720), metamorphic breakdown of muscovite has been identified (Eq. 2), which is a fluid creating process. In the same sample the lack of feldspars is interpreted as possible leaching of sodium and calcium from the plagioclase due to early hydrothermal activity. All of the baddeleyite bearing zircon grains studied in this sample also contain this darker zircon. Based on this, I suggest that the baddeleyite bearing zircon grains in this sample have been exposed to sodium and calcium rich (strongly alkaline) fluids during the metamorphism, resulting in leaching of silica and enrichment in sodium, calcium and immobile elements (such as uranium and hafnium). Such a scenario is indeed compatible with all observations in zircon grains with blobby baddeleyite occurrences, i.e. detectable Hf and U, silica decrease in partially affected zircon and occurrence of e.g. Na. Other elements could also give the impression of enrichment, but may be detected due to the changes in mass balance implied by this model.

4.4 Possible explanations

Here I propose a preliminary explanation for each of the two end-member types of occurrences. For the occurrences of baddeleyite that are concordant with the primary zonation, I suggest that variation in silica activity in the magma is the cause for the presence of baddeleyite. This would make the magma crystallise zircon when the silica activity is high and baddeleyite when the magma is temporarily or locally silica undersaturated. In contrast, I suggest that the occurrences of patchy irregular domains are due to later hydrothermal alteration of the zircon grains. This model is supported by the fracture patterns associated with this type of occurrence of baddeleyite, by their anheadral habitus, and geochemical characteristics.

5 What next?

To further investigate this phenomenon and reach a more solid theory, some future work is needed. For example, precise and accurate U-Pb geochronology of zircon and baddeleyite domains will provide important clues to the origin and timing of baddeleyite generating events. Linking baddeleyite formation with metamorphism will probably provide important clues about metamorphic fluid chemistry and reactions during

$$2(KAl_3Si_3O_{10}(OH)_2) + 2H^+ \rightleftharpoons 3(Al_2SiO_5) + 3(SiO_2) + 2K^+ + 3(H_2O) \quad \textbf{[Eq. 2]}$$

various metamorphic stages. U-Pb age data should ideally be linked with O-Hf data, which might provide further evidence on the origin and on metamorphic fluids.

6 Conclusions

- This phenomenon is present as two types of occurrences, possibly originated from different processes.
- Possible explanations of the phenomenon are variation in silica activity as a primary process and later hydrothermal alteration as a secondary process.

7 Acknowledgements

First of all I would like to thank my supervisor Anders Scherstén for valuable comments, insights and suggestions. Nevertheless I thank my co-supervisors at GEUS, Nynke Keulen and Thomas Kokfelt, for providing of the material and important insights to SEM-EDS and LA-ICPMS U-Pb geochronology, as well as rewarding discussions.

8 References

Champness, P.E., 1995: Analytical electron microscopy. *In* Potts, P.J., Bowles, J.F.W., Reed, S.J.B. & Cave, M.R. (editors): Microprobe Techniques in the Earth Sciences. *Mineralogical Society Series 6*, 91-139.

Friend, C.R.L. & Nutman, A.P., 2005: New pieces to the Archaean terrane jigsaw puzzle in the Nuuk region, southern West Greenland: steps in transforming a simple insight into a complex regional tectonothermal model. *Journal of the Geological Society (London) 162*, 147-162.

Friend, C.R.L., Nutman, A.P., Baadsgaard, H., Kinny, P.D., McGregor, V.R., 1996: Timing of late Archaean terrane assembly, crustal thickening and granite emplacement in the Nuuk region, southern West Greenland. *Earth and Planetary Science Letters 142*, 353-365.

Hanmer, S., Hamilton, M.A. & Crowley, J.L., 2002: Geochronological constraints of Paleoarchean thrust-nappe and Neoarchean accretionary tectonics in southern West Greenland. *Tectonophysics 350*, 255-271.

Henriksen, N., 2008: *Geological History of Greenland: four billion years of Earth evolution*. Geological Survey of Denmark and Greenland (GEUS), Copenhagen. 272 pp.

Janoušek, V., Farrow, C. M. & Erban, V., 2006: Interpretation of whole-rock geochemical data in igneous geochemistry: introducing Geochemical Data Toolkit (GCDkit). *Journal of Petrology 47*, 1255-1259.

Keulen, N., Scherstén, A., Schumacher, J.C., Næraa, T. & Windley, B.F., 2009: Geological observations in the southern West Greenland basement from Ameralik to Frederikshåb Isblink in 2008. *Geological Survey of Denmark and Greenland Bulletin 17*, 49-52.

Long, J.V.P., 1995: Microanalysis from the 1950 to the 1990s. *In* Potts, P.J., Bowles, J.F.W., Reed, S.J.B. & Cave, M.R. (editors): Microprobe Techniques in the Earth Sciences. *Mineralogical Society Series 6*, 1-48.

Næraa, T. & Scherstén, A., 2008: New zircon ages from the Tasiusarsuaq terrane, southern West Greenland. *Geological Survey of Denmark and Greenland Bulletin 15*, 73-76.

Nutman, A.P., Friend, C.R.L., Barker, S.L.L., McGregor, V.R., 2004: Inventory and assessment of Palaeoarchaean gneiss terrains and detrital zircons in southern West Greenland. *Precambrian Research 135*, 281-314.

Pidgeon, R.T. & Kalsbeek, F., 1978: Dating of igneous and metamorphic events in the Fiskenaesset region of southern west Greenland. *Canadian Journal of Earth Sciences 15*, 2021-2025.

Reed, S.J.B, 1995: Electron microprobe microanalysis. *In* Potts, P.J., Bowles, J.F.W., Reed, S.J.B. & Cave, M.R. (editors): Microprobe Techniques in the Earth Sciences. *Mineralogical Society Series 6*, 49-89.

Schiøtte, L., Compston, W. & Bridgewater, D., 1989: U-Pb single-zircon age for the Tinissaq gneiss of southern West Greenland: a controversy resolved. *Chemical Geology 79*, 21-30.

Windley, B.F. & Garde, A.A., 2009: Arc-generated blocks with crustal sections in the North Atlantic craton of West Greenland: crustal growth in the Archean with modern analogues. *Earth-Science Reviews 93*, 1-30.

Appendix 1: Thin section overveiws

Thin section 468720

Thin section 508602

Thin section 510155

Thin section 512013

Thin section 512028

Thin section 512075

Appendix 2: Photos of zircon grains in thin section

Thin section 468720b

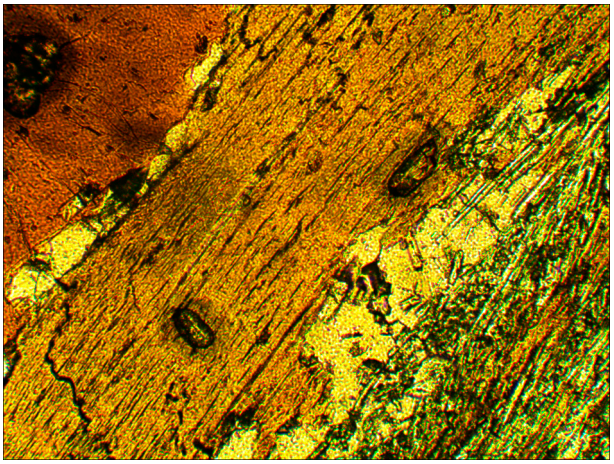
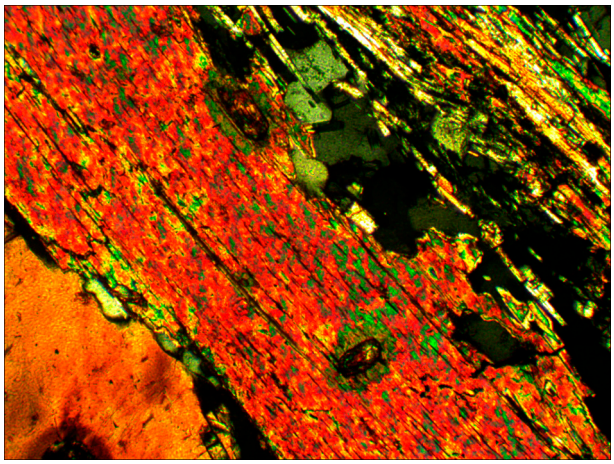

Photo number 1 for thin section 468720b showing zircon grains in biotite. To the left, under plane polarised light. To the right, cross polarised light.


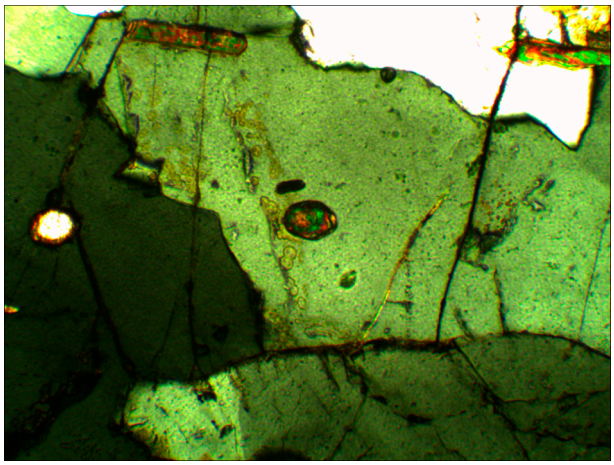

Photo number 2 for thin section 468720b showing a zircon grain in quartz. To the left, under plane polarised light. To the right, cross polarised light.

Thin section 508602

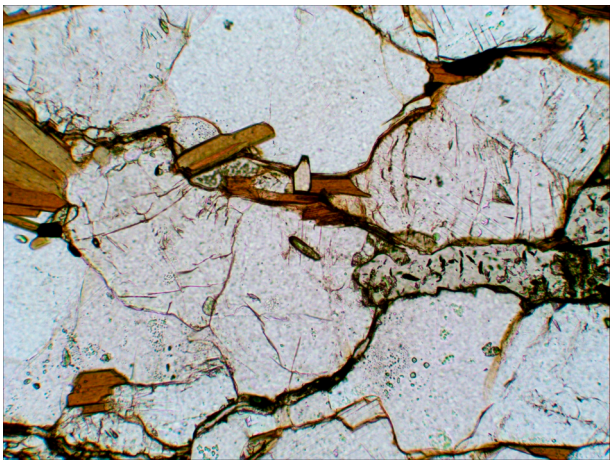
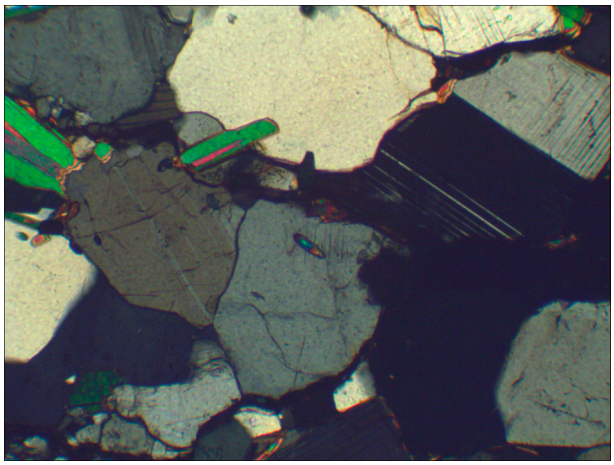

Photo number 1 for thin section 508602 showing a zircon grain in plagioclase. To the left, under plane polarised light. To the right, cross polarised light.

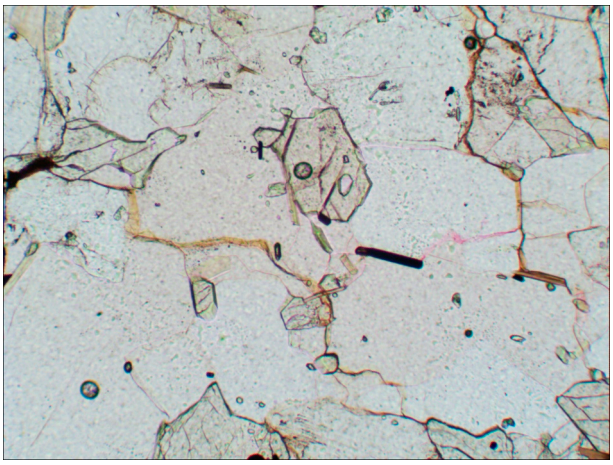
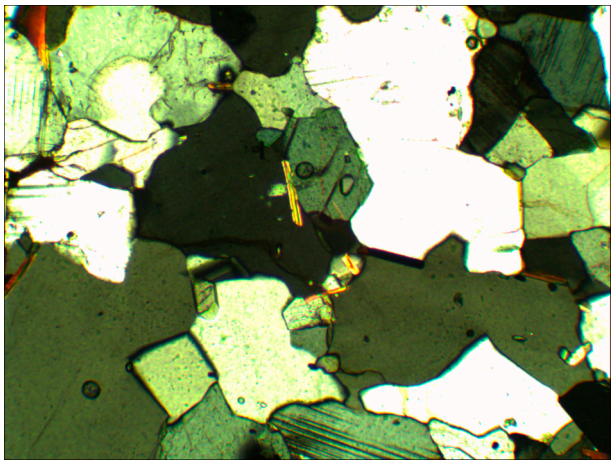

Photo number 2 for thin section 508602 showing a zircon grain in quartz. To the left, under plane polarised light. To the right, cross polarised light.

Thin section 510155

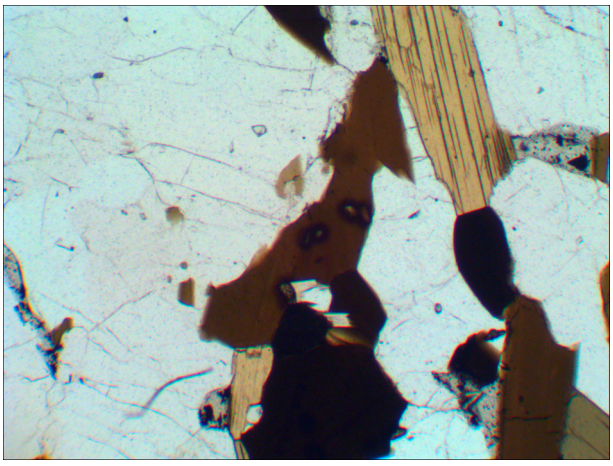
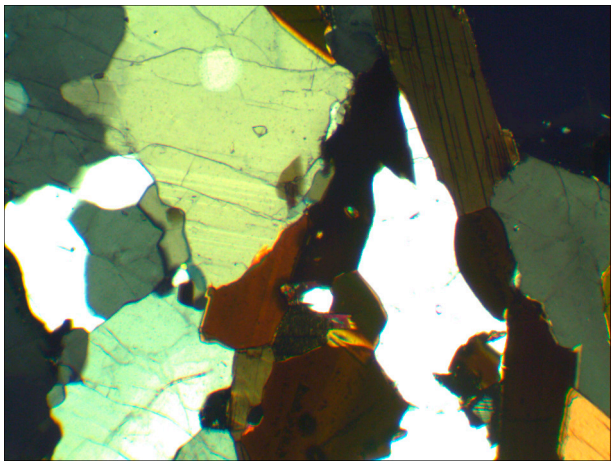

Photo number 1 for thin section 510155 showing zircon grains in biotite. To the left, under plane polarised light. To the right, cross polarised light.

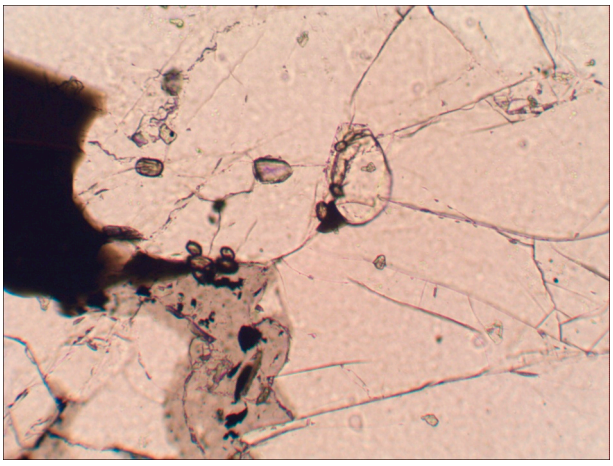
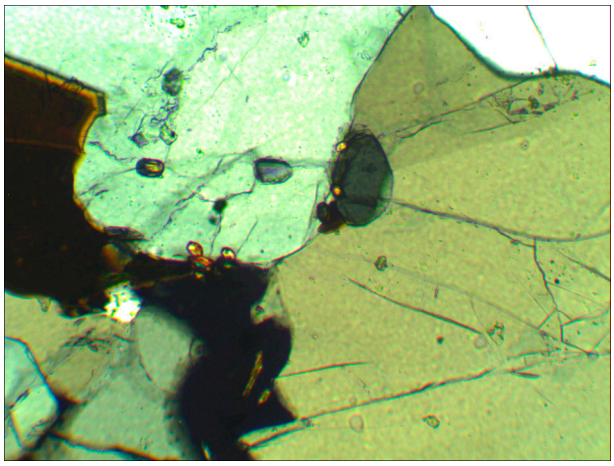

Photo number 2 for thin section 510155 showing zircon grains in quartz. To the left, under plane polarised light. To the right, cross polarised light.

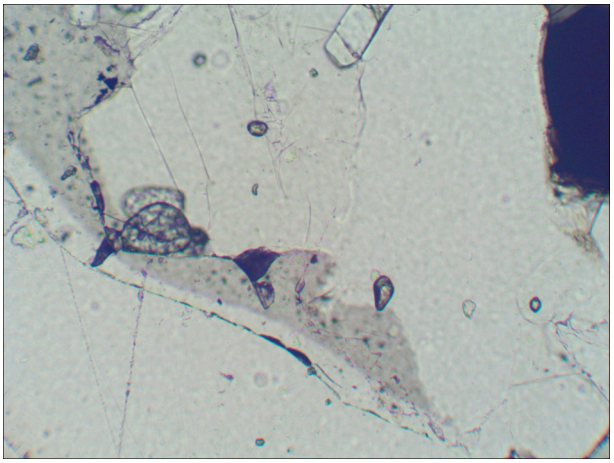
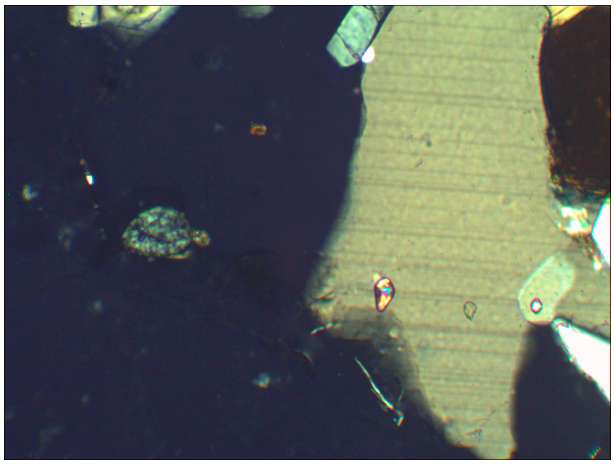

Photo number 3 for thin section 510155 showing a zircon grain in plagioclase. To the left, under plane polarised light. To the right, cross polarised light.

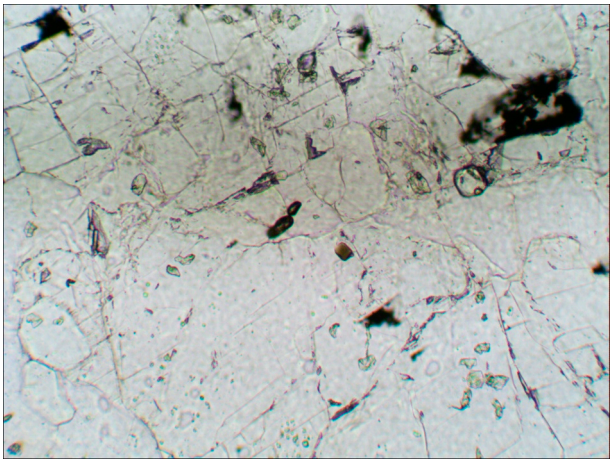
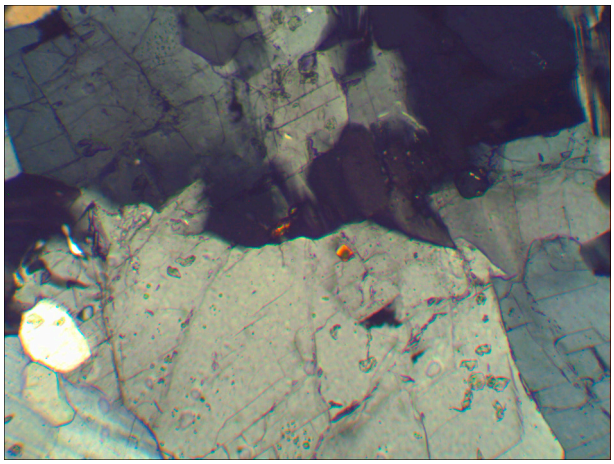

Photo number 4 for thin section 510155 showing a zircon grain in K-feldspar. To the left, under plane polarised light. To the right, cross polarised light.

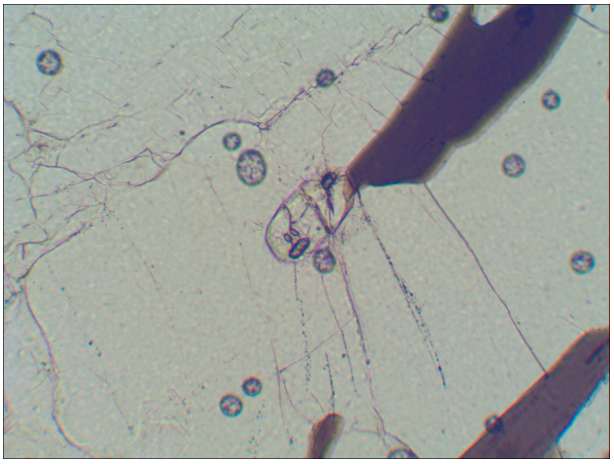
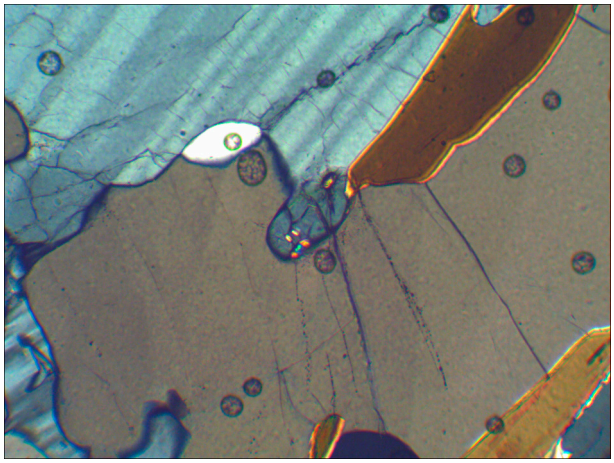

Photo number 5 for thin section 510155 showing zircon grains in apatite. To the left, under plane polarised light. To the right, cross polarised light.

Thin section 512013

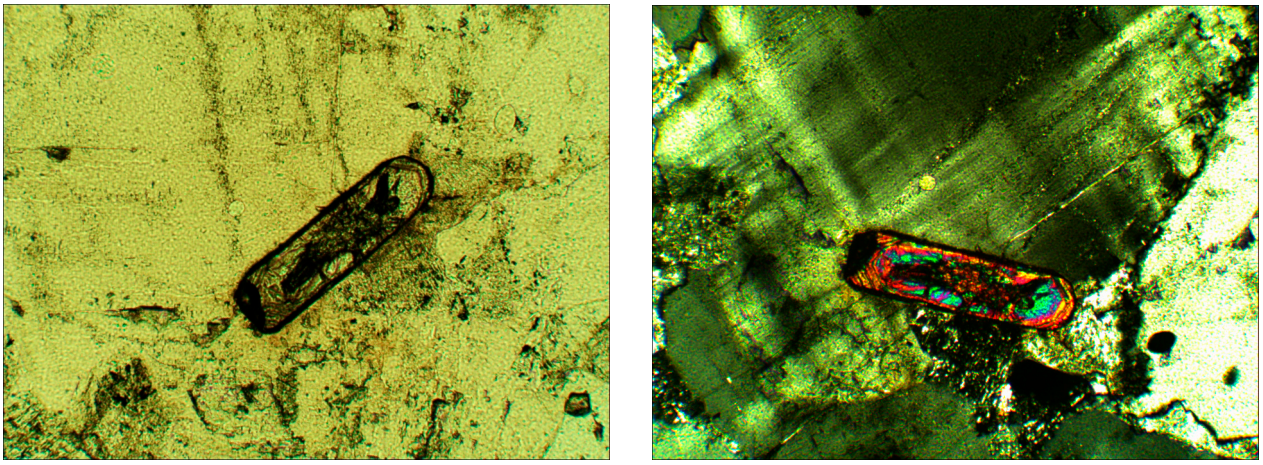

Photo number 1 for thin section 512013 showing a zircon grain in K-feldspar. To the left, under plane polarised light. To the right, cross polarised light.

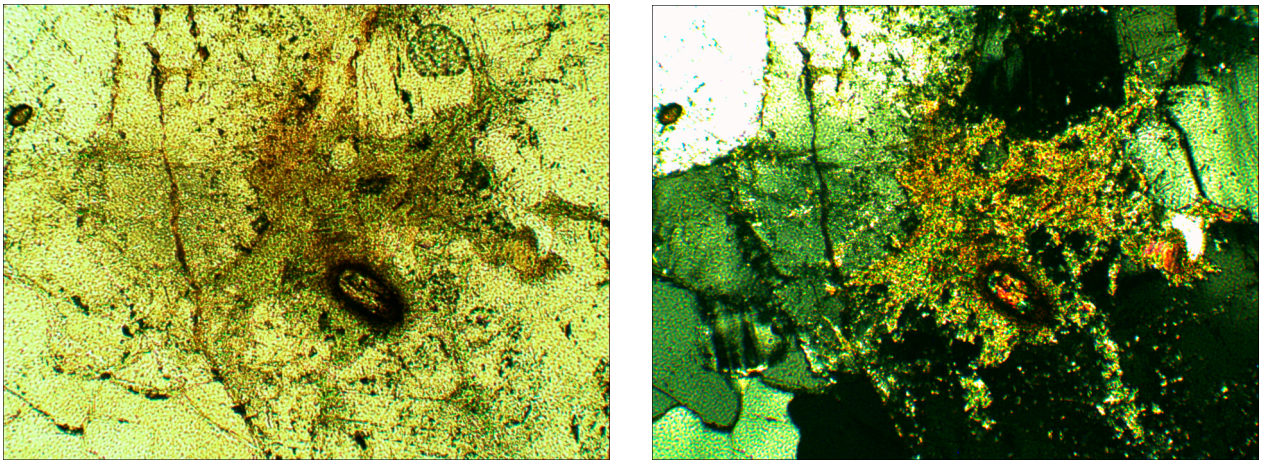

Photo number 2 for thin section 512013 showing a zircon grain in chlorite. To the left, under plane polarised light. To the right, cross polarised light.

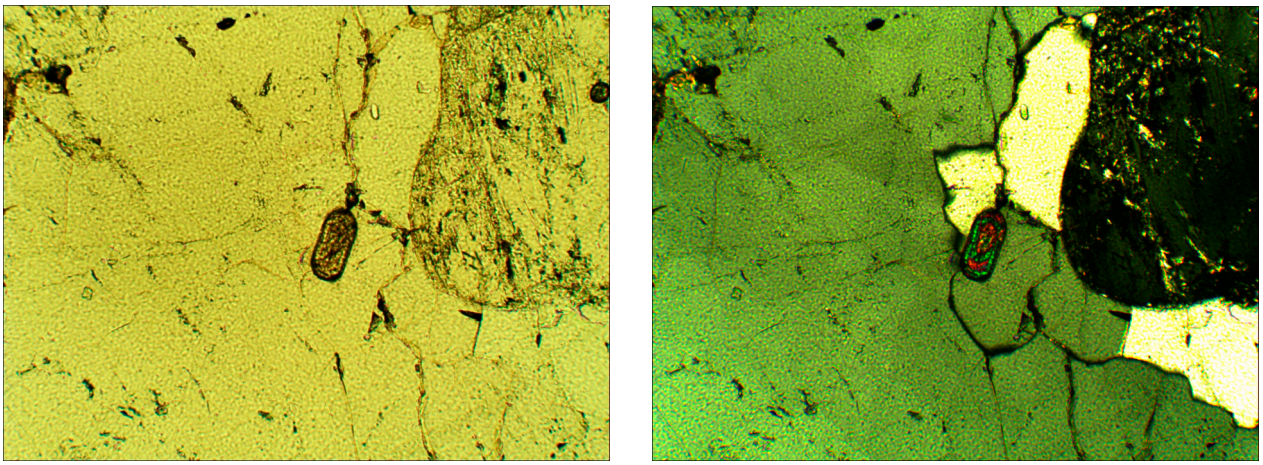

Photo number 3 for thin section 512013 showing a zircon grain in quartz. To the left, under plane polarised light. To the right, cross polarised light.

Thin section 512028

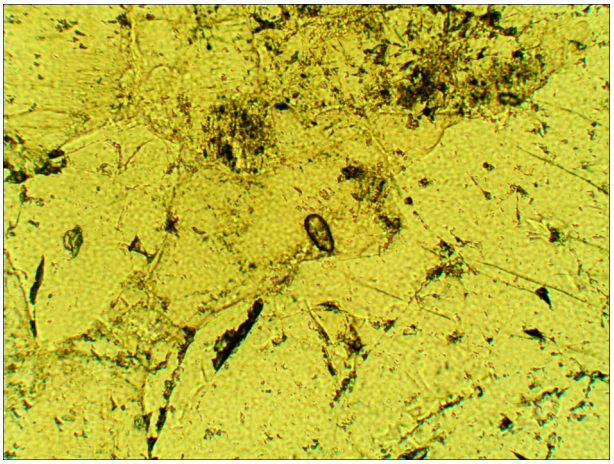
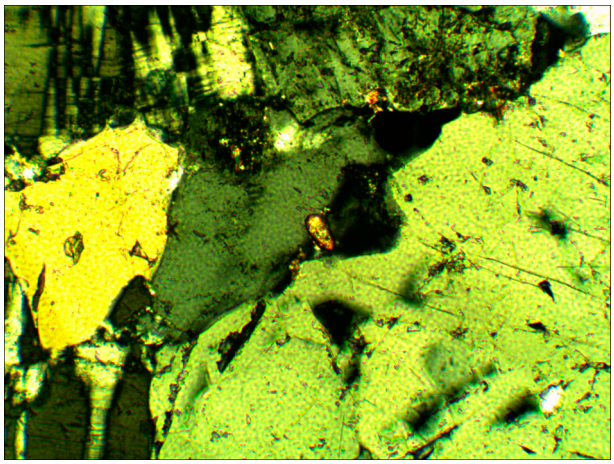

Photo number 1 for thin section 512028 showing a zircon grain in quartz. To the left, under plane polarised light. To the right, cross polarised light.

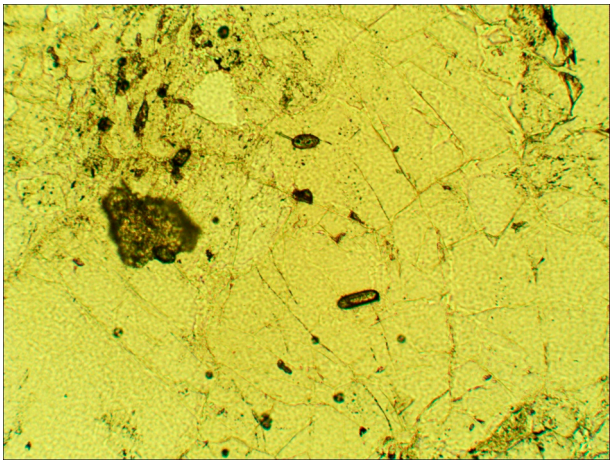
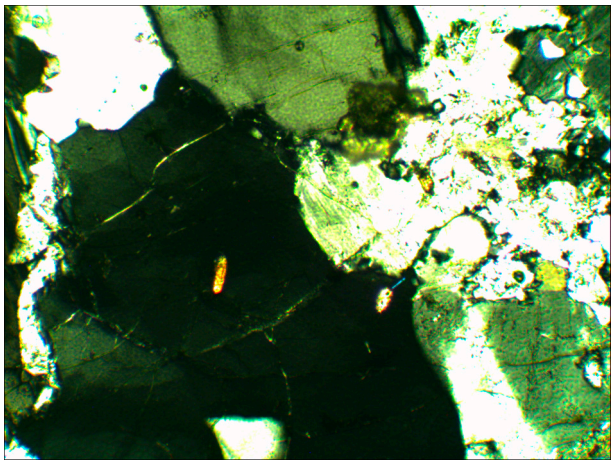

Photo number 2 for thin section 512028 showing a zircon grain in plagioclase. To the left, under plane polarised light. To the right, cross polarised light.

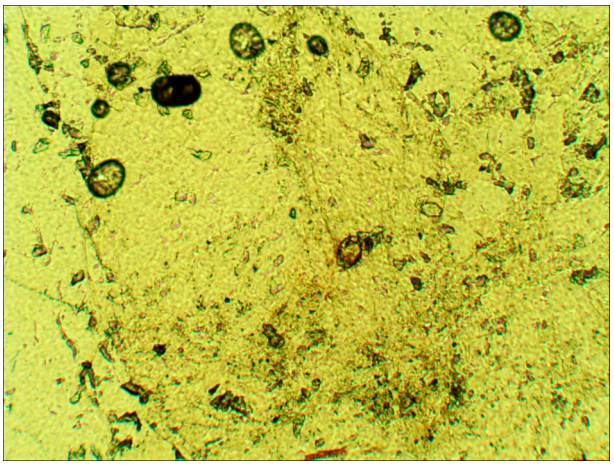
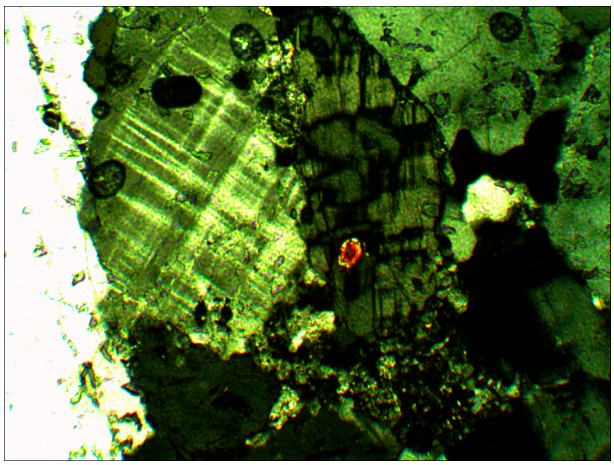

Photo number 3 for thin section 512028 showing a zircon grain in K-feldspar. To the left, under plane polarised light. To the right, cross polarised light.

Thin section 512075

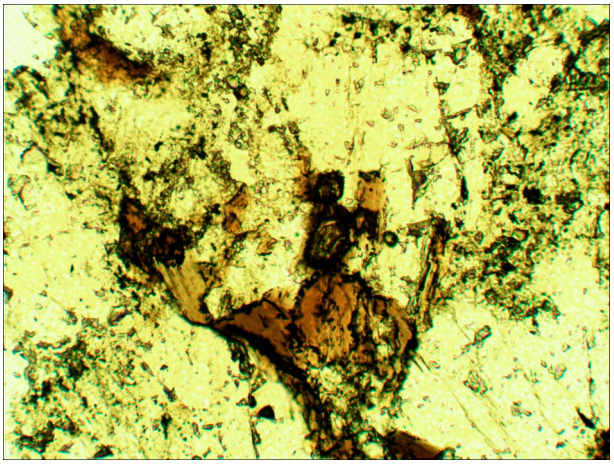
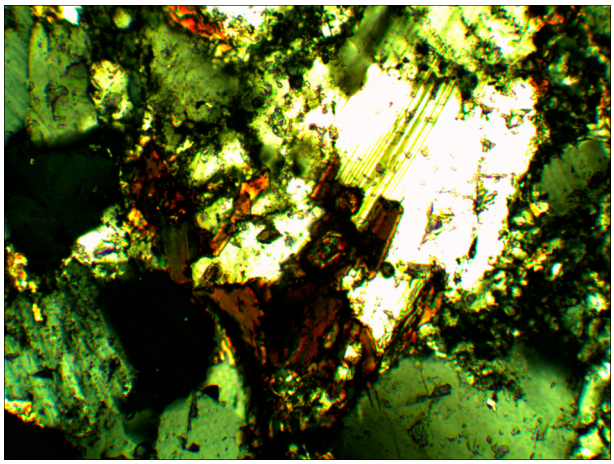

Photo number 1 for thin section 512075 showing a zircon grain in biotite. To the left, under plane polarised light. To the right, cross polarised light.

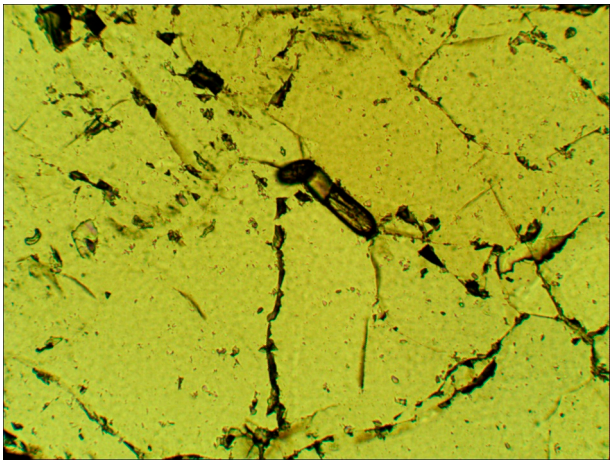
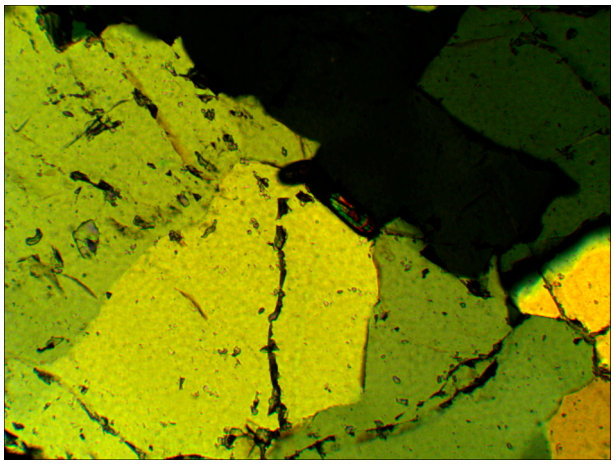

Photo number 2 for thin section 512075 showing a zircon grain in quartz. To the left, under plane polarised light. To the right, cross polarised light.

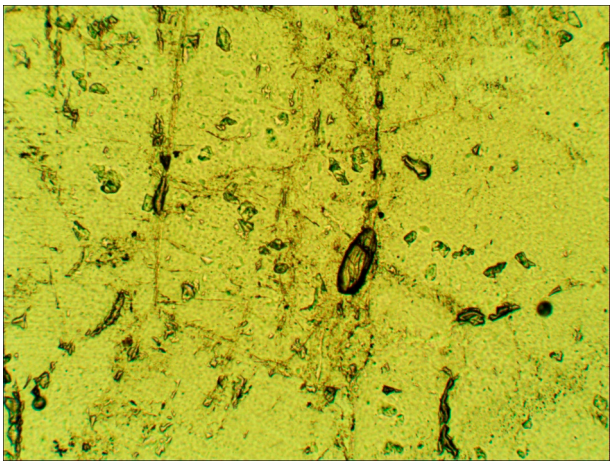
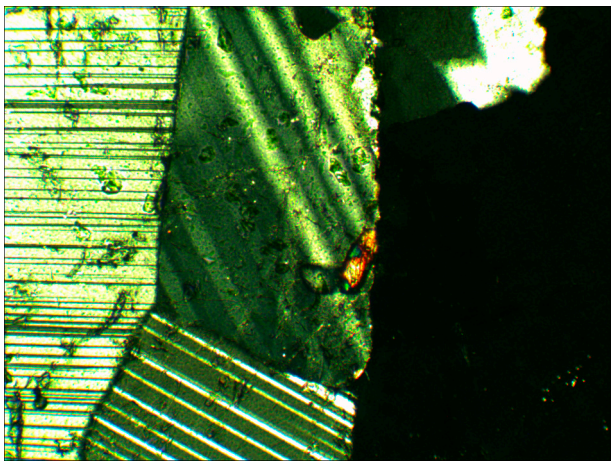

Photo number 3 for thin section 512075 showing a zircon grain in plagioclase. To the left, under plane polarised light. To the right, cross polarised light.

Appendix 2: EDS-data

N.B.: For almost all of the baddeleyite domains and some of the zircon zones, the spot size is larger than the analysed area. Therefore analyses can be composite analyses of several minerals, zones or domains. Analyses of baddeleyite domains are marked with red numbers.

Zircon mount 510155

Zircon area 1

	1	2	3	4	5
Al				0.02	
Si	0.94	0.91	0.92	0.08	0.93
Ca		0.03	0.03	0.02	
Fe		0.02	0.03	0.05	
Zr	1.06	1.05	1.04	0.86	1.07
Hf		0.01	0.01	0.02	
U				0.01	
O	4	4	4	2	4
∑ cat ions	2	2.02	2.03	1.03	2

Zircon area 2

	1	2	3	4	5	6
Al	0.03	0.02			0.08	0.02
Si	0.16	0.91	0.93	0.92	0.79	0.89
Ca	0.05	0.01			0.1	0.03
Ti	0.07				0.03	
Fe	0.04	0.03			0.03	
Zr	0.69	0.99	1.07	1.06	1.01	1.08
Hf	0.02	0.02			0.03	
U	0.01					
Nd					0.01	
Na				0.07		
O	2	4	4	4	4	4
∑ cat ions	1.05	2.07	2	2.05	2.09	2.02

Zircon area 3

	1	2	3	4
Al	0.03			
Si	0.21	0.9	0.93	0.92
Ca	0.05	0.1		
Fe	0.05	0.04		
Zr	0.70	1.01	1.06	1.08
Hf	0.02	0.02		
U	0.01			
Na			0.08	
Cl		0.01		
O	2	3.99	4	4
∑ cat ions	1.05	2.06	2.06	2

Zircon area 4

	1	2	3	4	5
Al	0.04	0.03			0.41
Si	0.32	0.26	0.89	0.92	1.03
Ca	0.05	0.05	0.09		
Ti	0.01	0.01			
Fe	0.03	0.04	0.04		0.43
Zr	0.59	0.63	1.03	1.08	0.42
Hf	0.03	0.03			
U	0.01				
Cl			0.01		
Mg					0.03
K					0.03
O	2	4	3.99		1
∑ cat ions	1.05	1.05	2.06	2	2.35

Zircon mount 512028

Zircon area 1a

	1	2	3	4	5	6
Al	0.04					0.01
Si	0.14	0.88	0.88	0.88	0.84	0.88
Ca	0.03				0.04	0.01
Fe	0.02				0.03	
Zr	0.77	1.12	1.12	1.12	1.11	1.11
Na					0.03	
Cl	0.02				0.02	
O	1.95	4	4	4	3.98	4
∑ cat ions	1.03	2	2	2	2.05	2.01

Zircon area 1b

	1	2	3	4	5	6
Al	0.03			0.02	0.03	
Si	0.10	0.88	0.88	0.78	0.19	0.88
Ca	0.02			0.06	0.03	1.12
Fe	0.04			0.02	0.03	
Zr	0.86	1.12	1.12	1.15	0.78	
Na				0.02		
Cl				0.02		
O	2	4	4	3.98	2	4
∑ cat ions	1.03	2	2	2.05	1.03	2

Zircon area 2

	1	2	3	4	5	6
Al	0.03			0.02	0.05	
Si	0.10	0.88	0.88	0.78	0.37	0.88
Ca	0.02			0.06	0.05	1.12
Fe	0.04			0.02	0.05	
Zr	0.86	1.12	1.12	1.15	1.55	
Na				0.02		
Cl				0.02		
O	2	4	4	3.98	4	4
∑ cat ions	1.03	2	2	2.05	2.06	2

Zircon area 3

	1	2	3	4	5	6
Al				0.17		0.04
Si	0.88	0.88	0.87	0.78	0.85	0.08
Ca				0.02	0.04	0.03
Fe				0.03	0.03	0.03
Zr	1.12	1.12	1.13	1.07	1.1	0.84
U						0.01
Na					0.03	
Cl					0.02	0.01
Mn						0.02
O	4	4	4	4	3.98	1.99
∑ cat ions	2	2	2	2.07	2.04	1.04

Zircon area 4

	1	2	3	4
Al	0.02			
Si	0.09	0.86	0.88	0.87
Ca	0.03	0.01		
Fe	0.02	0.02		
Zr	0.88	1.12	1.11	1.13
Na		0.04	0.04	
O	2	4	4	4
∑ cat ions	1.03	2.04	2.03	2

Zircon area 8

	1	2	3	4	5
Al	0.02	0.26	0.01	0.02	0.15
Si	1.98	0.53	1.96	0.93	1.54
Ca			0.01		
Zr		0.3	0.03	0.26	0.34
U				0.24	
Na	0.02				
K		0.05			0.04
Pb		1.93		0.08	
Yb			0.01		
Th				0.39	
O	4	4	4	4	4
∑ cat ions	2	3.07	2.01	1.93	2.07

Thin section 468720

Zircon area 1

	1	2	3	4	5	6
Al	0.02	0.01		0.03	0.02	
Si	0.07	0.25	0.88	0.83	0.07	1
Fe				0.03	0.01	
Zr	0.92	0.75	1.12	1.14	0.91	
O	2	2	4	4	2	2
∑ cat ions	1.01	1.01	2	2.02	1.01	1

Zircon area 2

	1	2	3	4	5	6	7	8
Al	0.04		0.02	0.11	0.1	0.7	1.30	
Si	0.35	0.87	0.21	0.77	0.76	0.7	2.68	1
Ca	0.02		0.01	0.03	0.03		0.30	
Fe	0.02		0.01	0.05	0.05	0.02		
Zr	0.64	1.13	0.77	1.1	1.12	0.87		
Na							0.76	
K							0.02	
O	2	4	2	4	4	2	8	2
∑ cat ions	1.03	2	1.02	2.07	2.06	1.03	5.04	1

Zircon area 3

	1	2	3	4	5
Al	0.02	0.21			1.30
Si	0.06	0.65	0.88	1	2.70
Ca		0.03			0.28
Ti	0.01				
Fe	0.03	0.68			
Zr	0.91	0.87	1.12		
Na					0.76
K					0.28
O	2	4	4	2	8
∑ cat ions	1.02	2.41	2	1	5.04

Zircon area 4

	1	2	3	4	5
Al	0.04		0.02	0.13	
Si	0.12	0.89	0.25	0.81	1
Fe	0.02		0.01		
Zr	0.85	1.11	0.74	1.1	
O	2	4	2	4	2
∑ cat ions	1.02	2	1.01	2.03	1

Zircon area 5

	1	2	3	4	5	6	7	8
Al	0.02		0.15	0.15		1.45	1.43	
Si	0.13	0.88	0.71	0.71	0.88	2.43	2.43	1
Ca	0.01		0.03	0.03				
Ti						0.18	0.15	
Fe	0.03		0.19	0.19		0.70	0.70	
Zr	0.84	1.12	1.07	1.07	1.12			
Cl						0.03		
Mg						1.45	1.48	
K						0.85	0.88	
Cr						0.08	0.03	
O	2	4	4	4	4	9.97	10	2
∑ cat ions	1.02	2	2.15	2.15	2	7.08	7.13	1

Thin section 510155

Zircon area 1		**Zircon area 2**		**Zircon area 3**
	1	1	2	1
Al	0.02	0.05	0.05	0.03
Si	0.45	0.2	0.19	0.17
Ca	0.01	0.01	0.01	0.05
Ti		0.04	0.04	0.07
Fe		0.04	0.04	0.04
Zr	0.55	0.70	0.72	0.70
Hf		0.02		0.02
U				0.01
Sc				0.01
O	2	2	2	2
∑ cat ions	1.01	1.04	1.04	1.05

Thin section 512028

Zircon area 1						**Zircon area 2**	
	1	2	3	4	5	1	2
Al	0.02	0.02		0.94	1.30	0.02	
Si	0.09	0.14	1	3.04	2.70	0.16	1
Ca		0.02			0.26	0.01	
Ti	0.03	0.03				0.02	
Fe	0.02	0.02				0.82	
Zr	0.87	0.80				0.01	
U	0.01	0.01					
Na					0.76		
K				1			
O	2	2	2	8	8	2	2
∑ cat ions	1.01	1.02	1	4.98	5.01	1.02	1

Thin section 512075

Zircon area 1							
	1	2	3	4	5	6	7
Al	0.04	0.03			0.32	0.02	1.48
Si	0.16	0.15	0.88	0.87	1	0.99	2.52
Ca	0.03	0.03			0.03		0.46
Ti	0.02						
Fe	0.02	0.02					
Zr	0.77	0.80	1.12	1.13	0.71		
Hf	0.01						
U		0.01					
Na					0.05		0.56
K					0.09		
Yb						0.01	
O	2	2	4	4	4	2	8
∑ cat ions	1.03	1.03	2	2	2.2	1.02	5.02

Appendix 3. EDS line scans

Zircon mount 510155

Zircon area 2

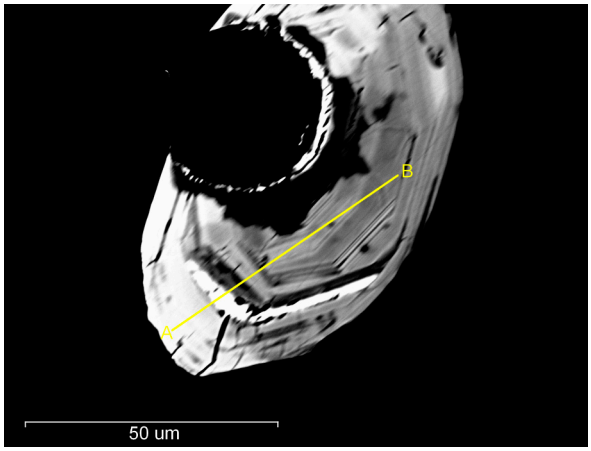

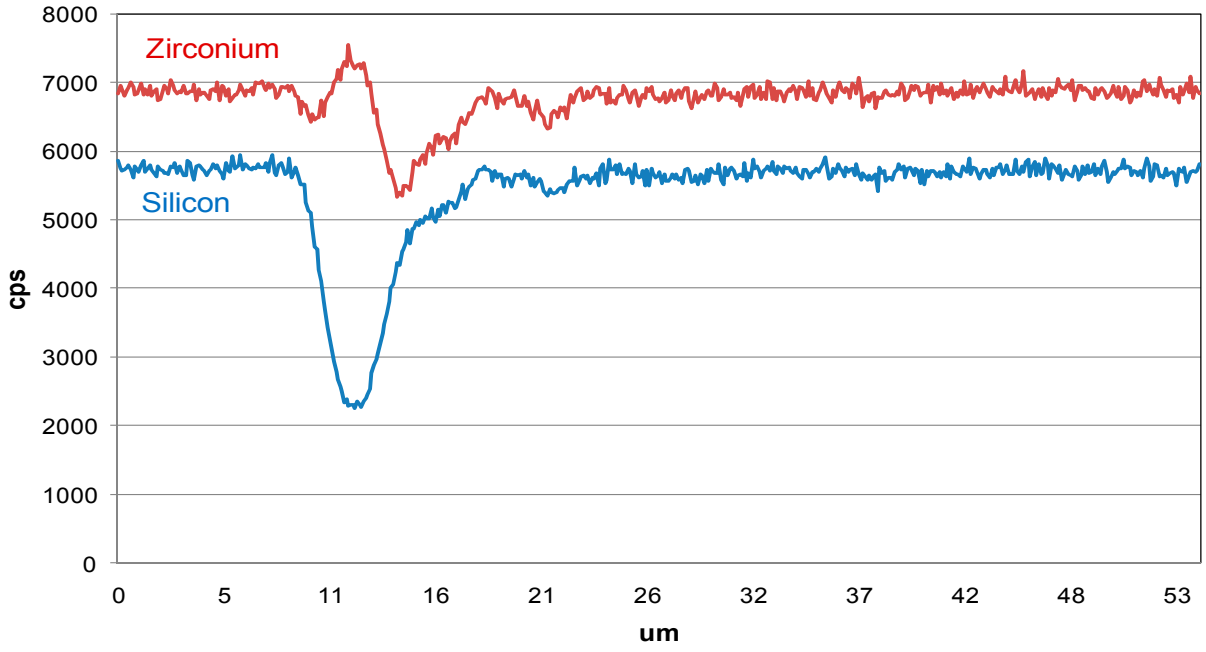

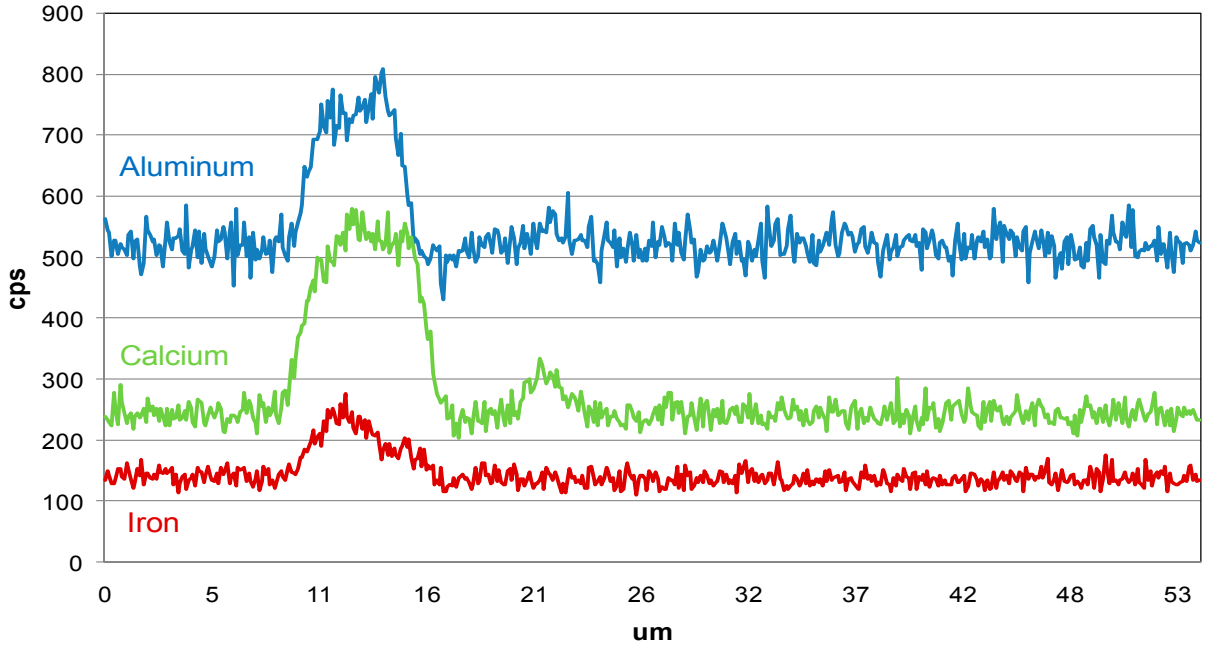

Zircon mount 510155
Zircon area 4

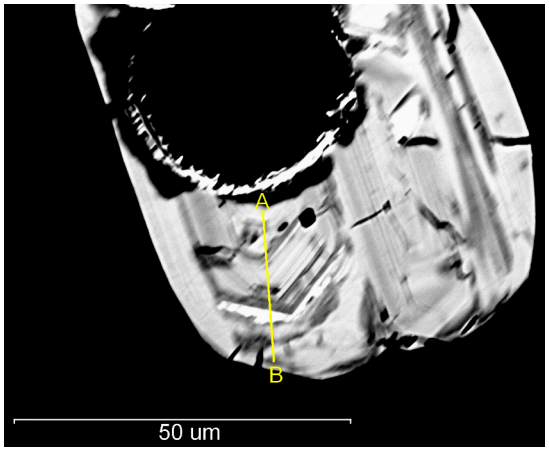

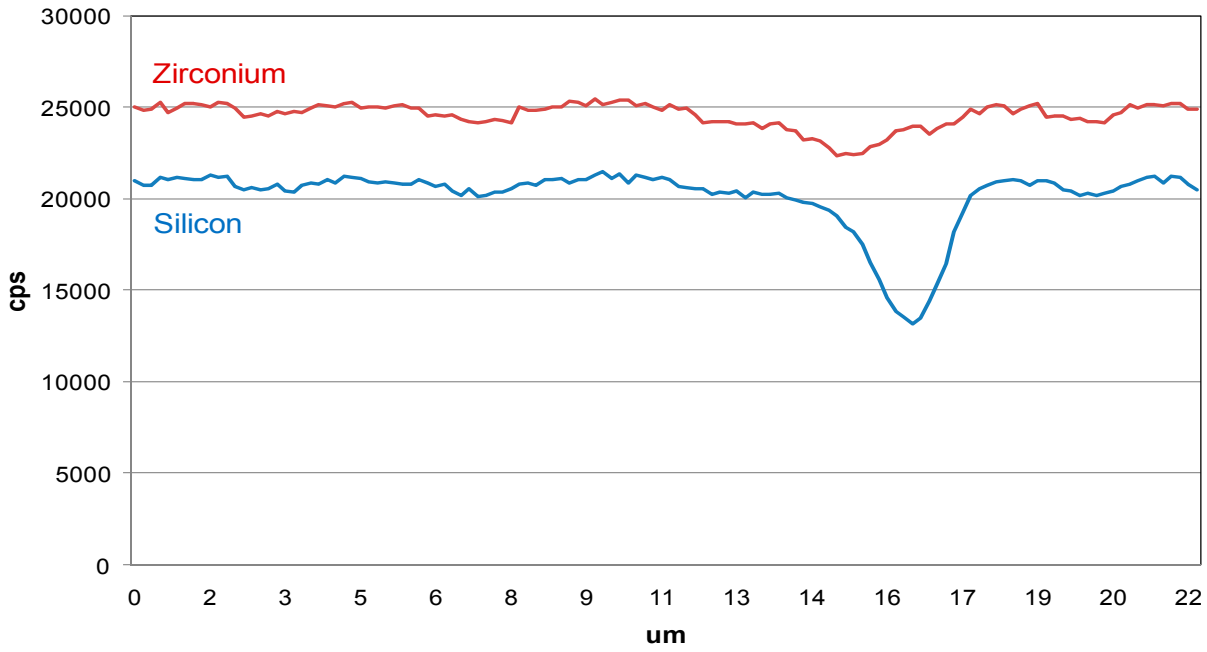

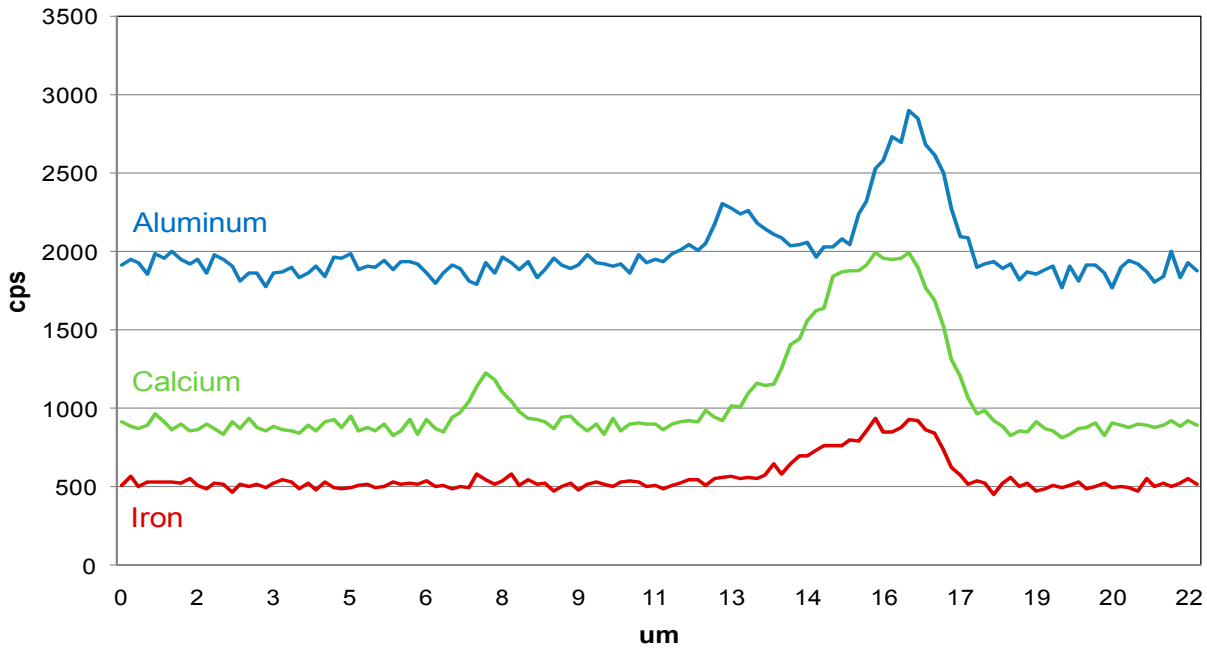

Zircon mount 512028
Zircon area 1A

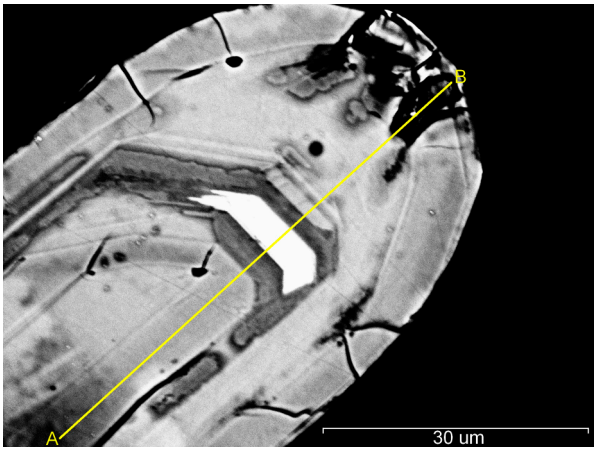

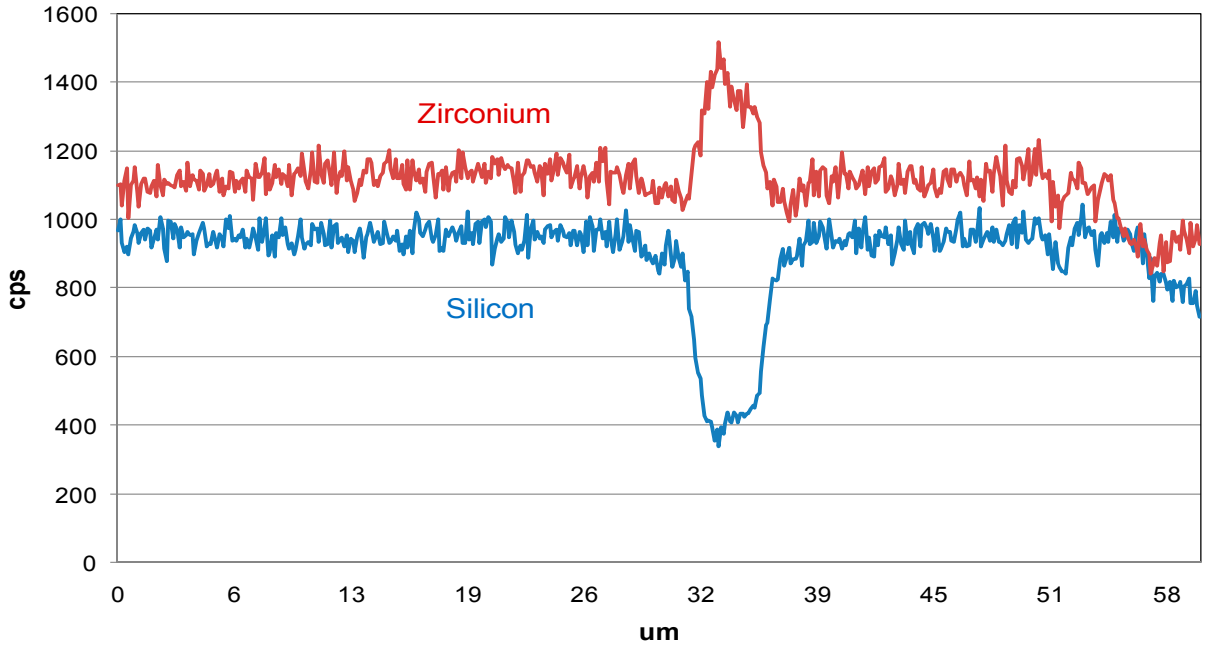

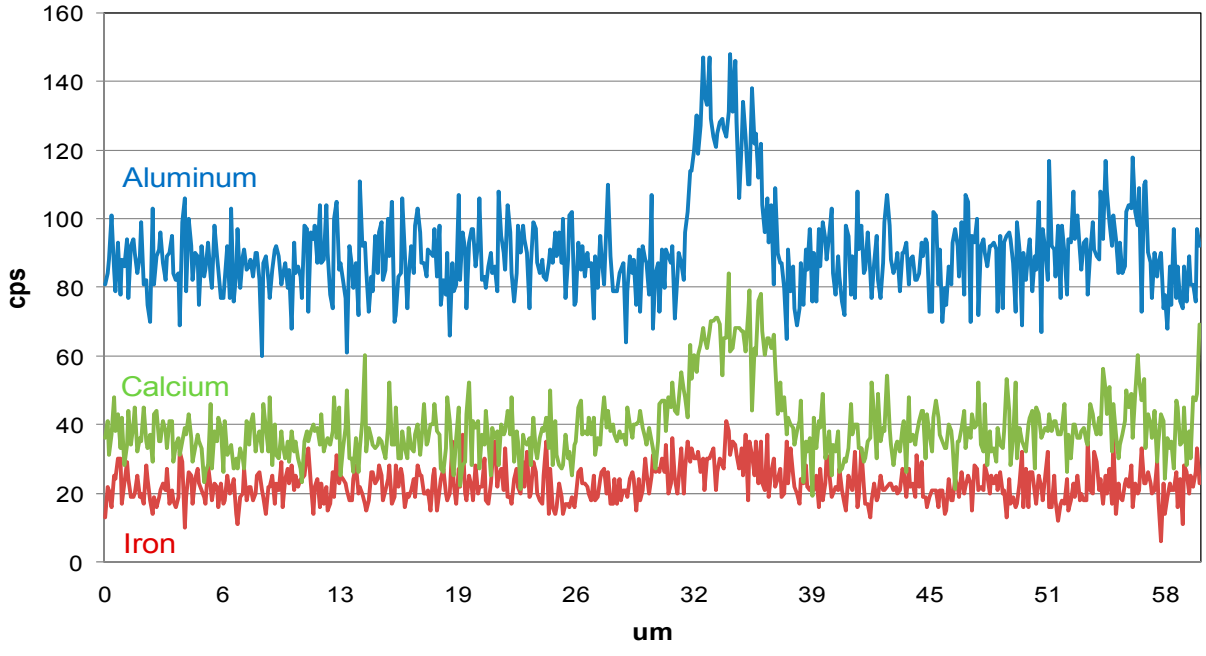

Zircon mount 512028
Zircon area 1B

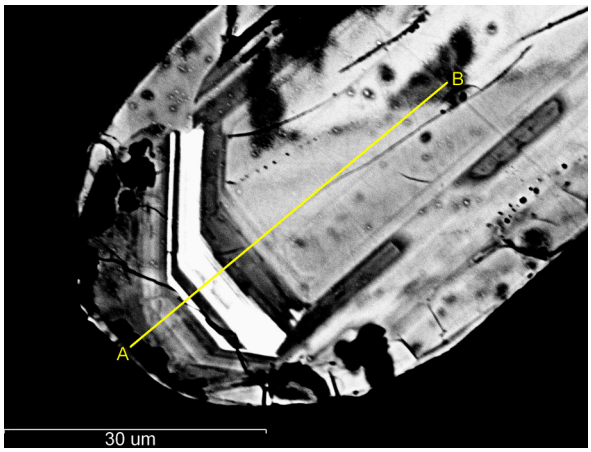

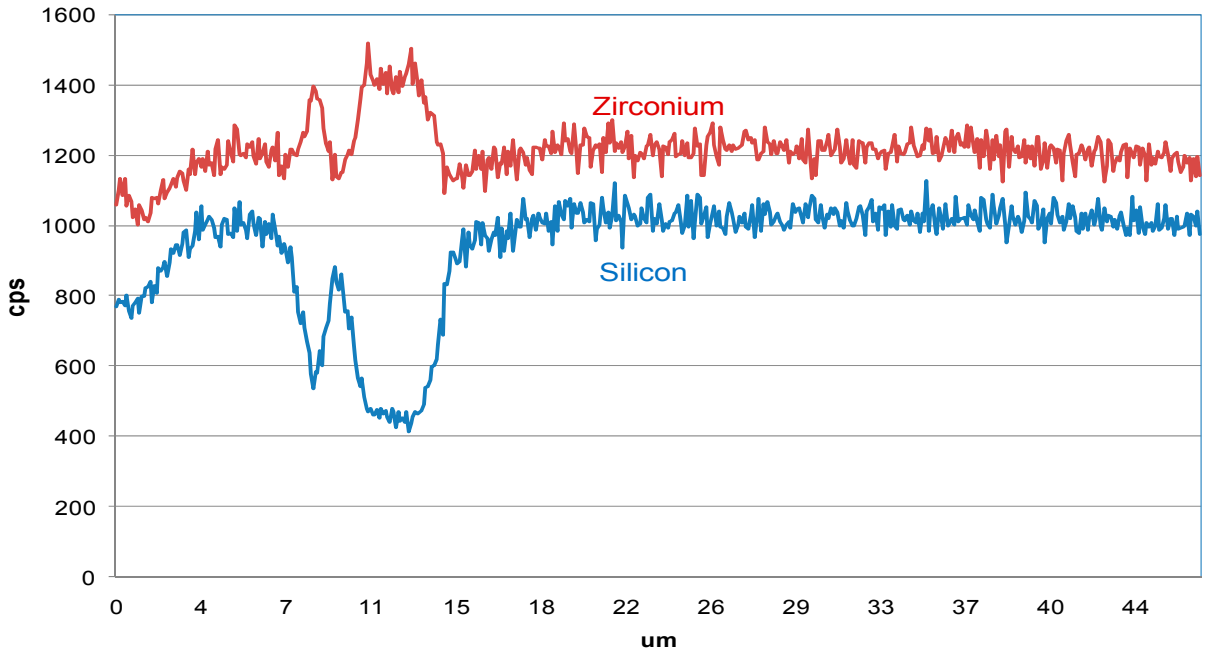

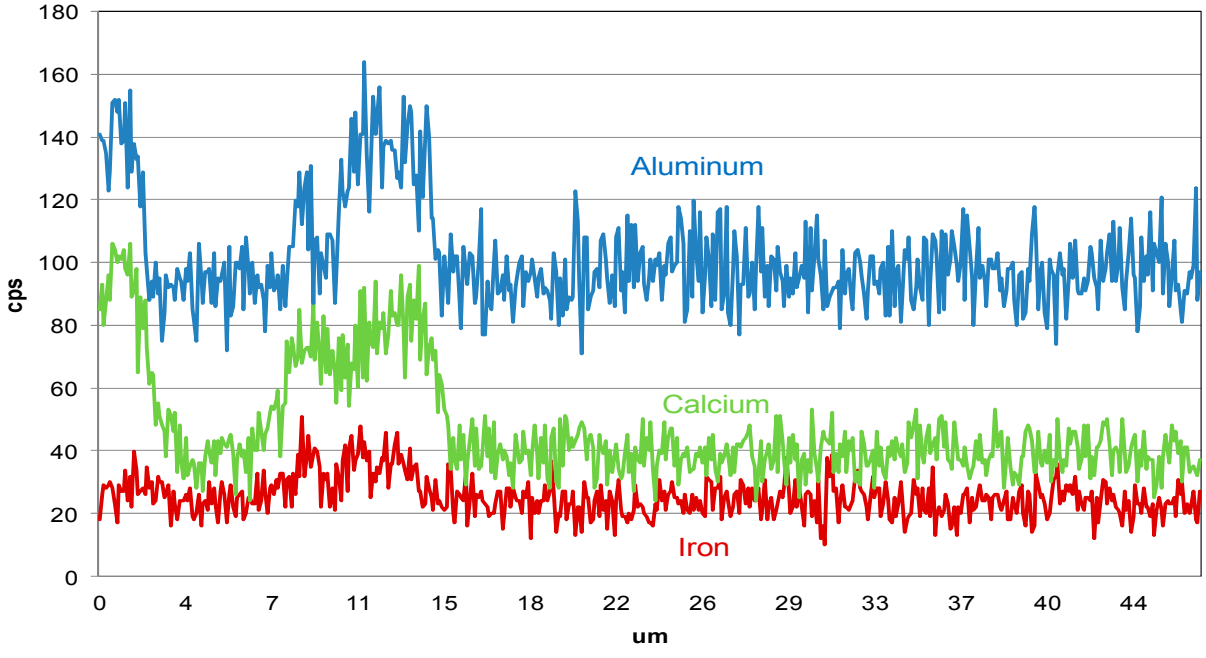

Zircon mount 512028
Zircon area 2

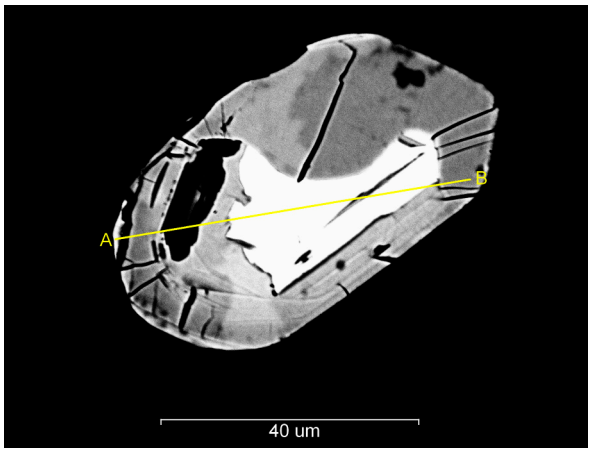

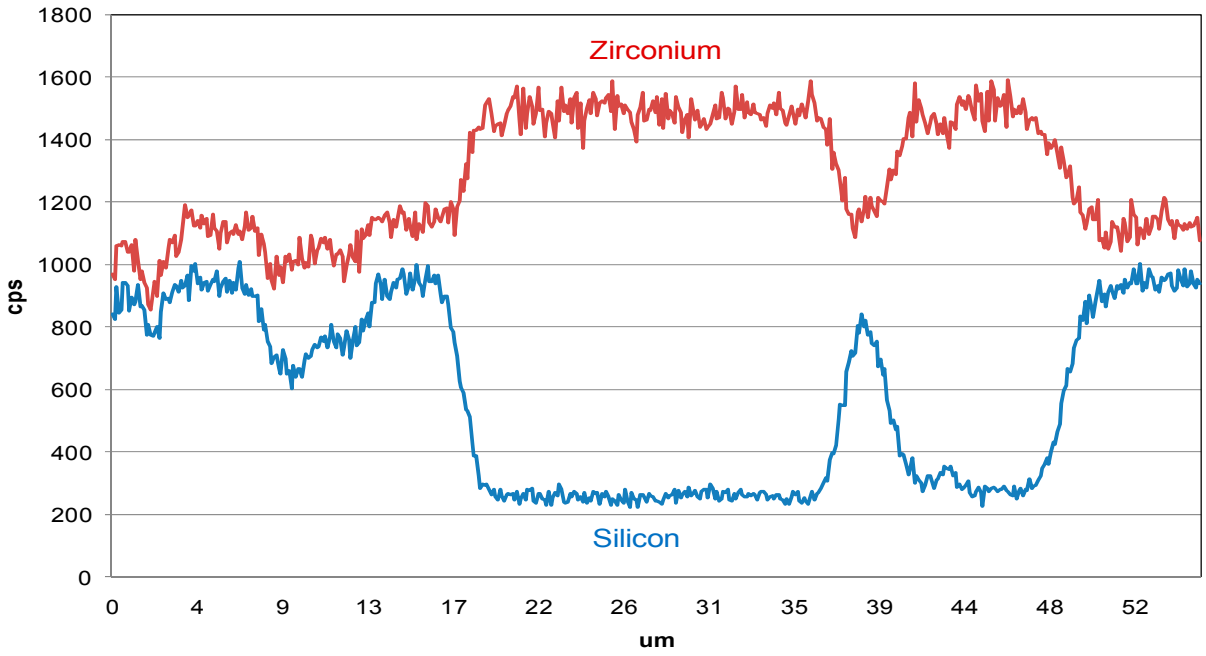

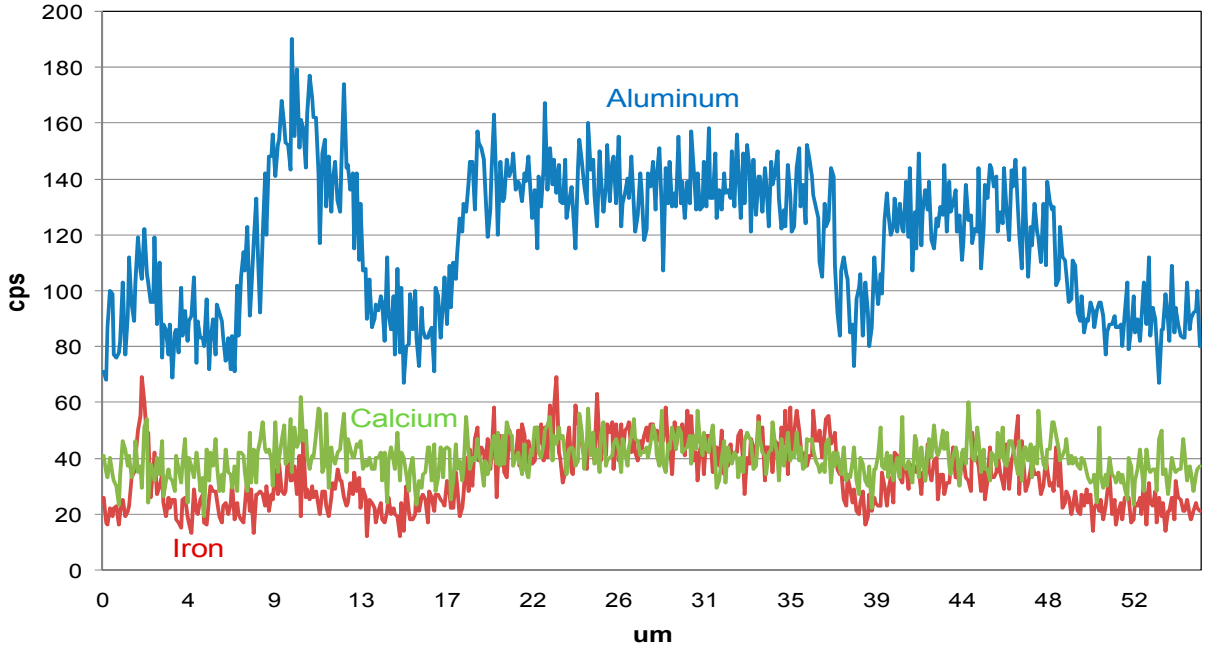

Zircon mount 512028
Zircon area 3

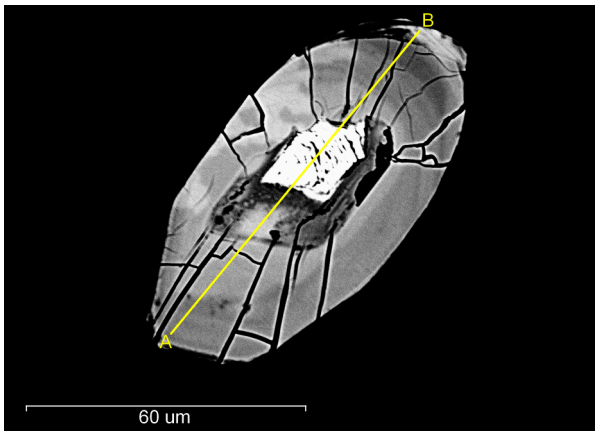

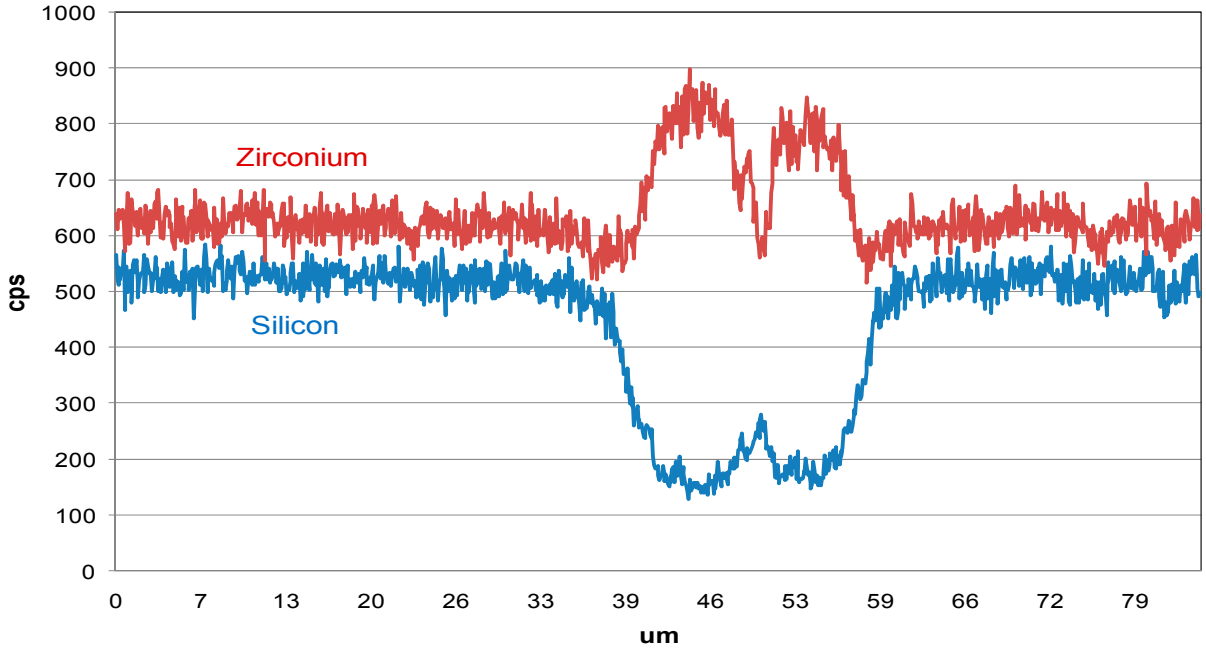

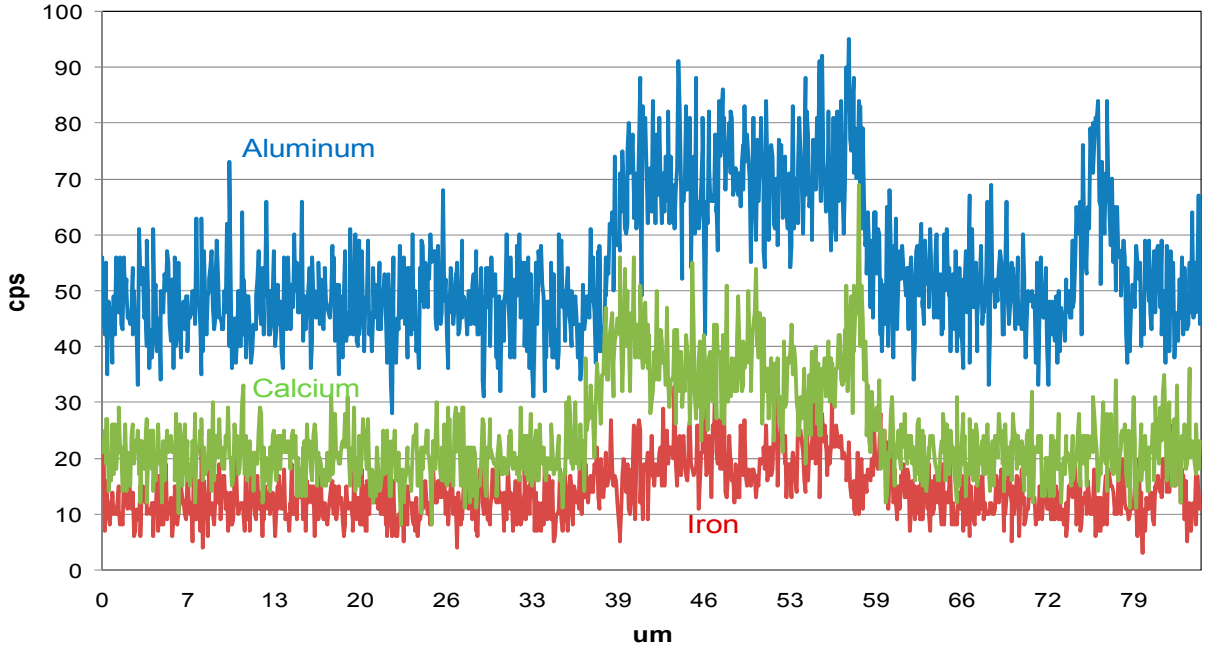

Zircon mount 512028
Zircon area 4

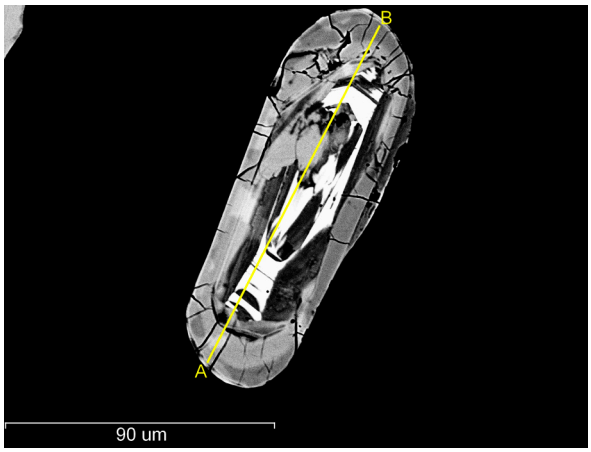

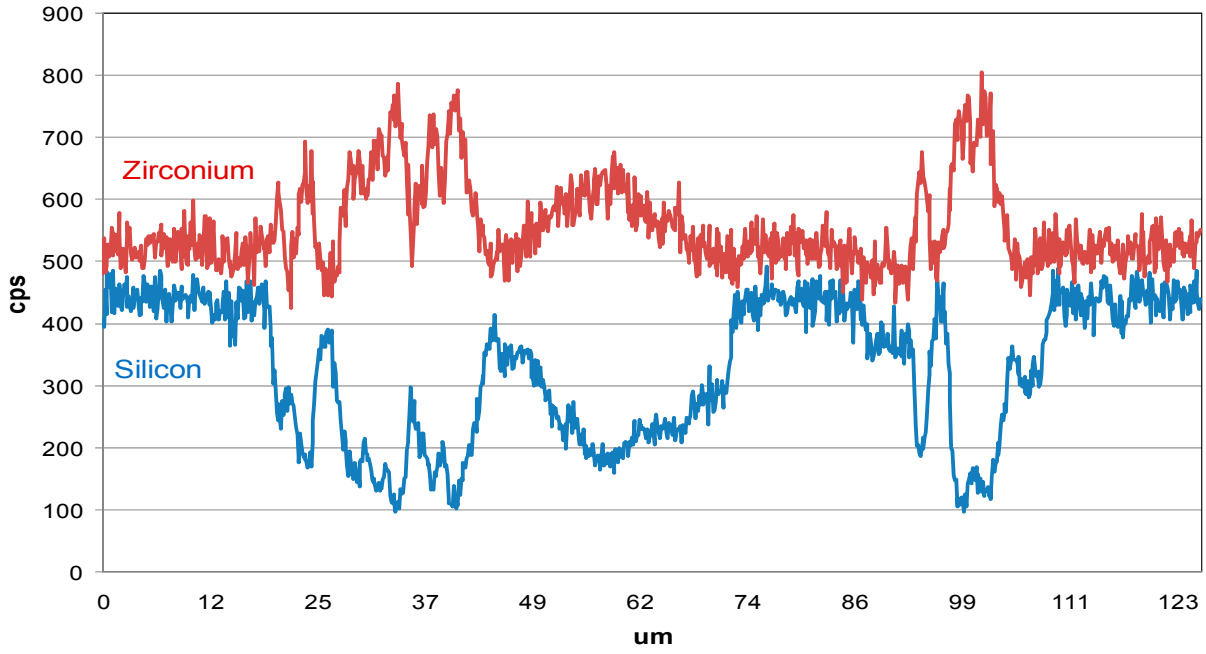

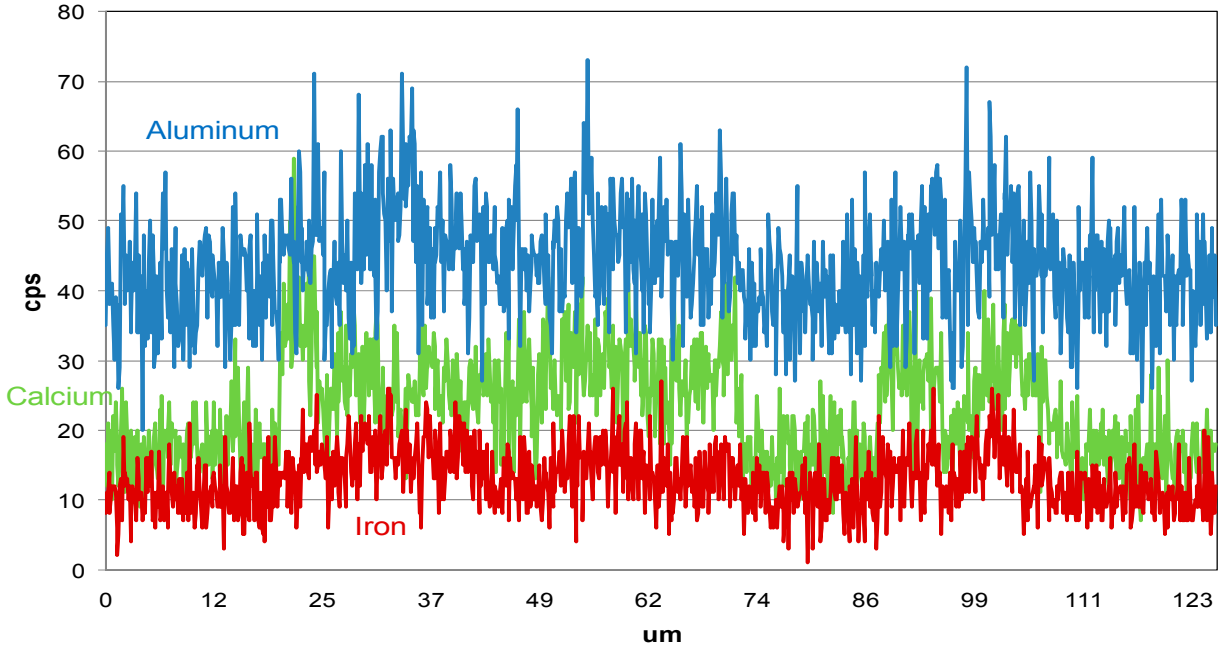

Thin section 468720
Zircon area 1

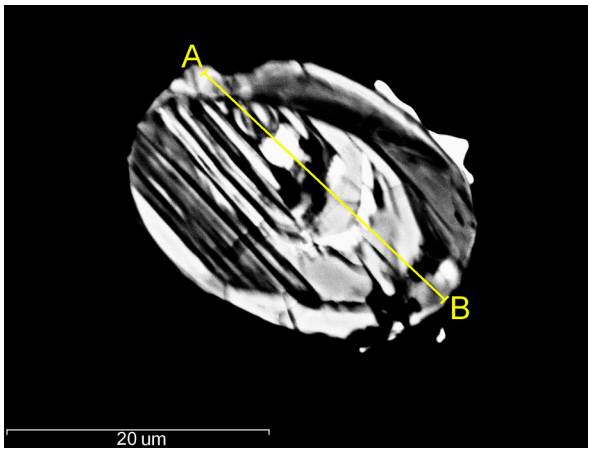

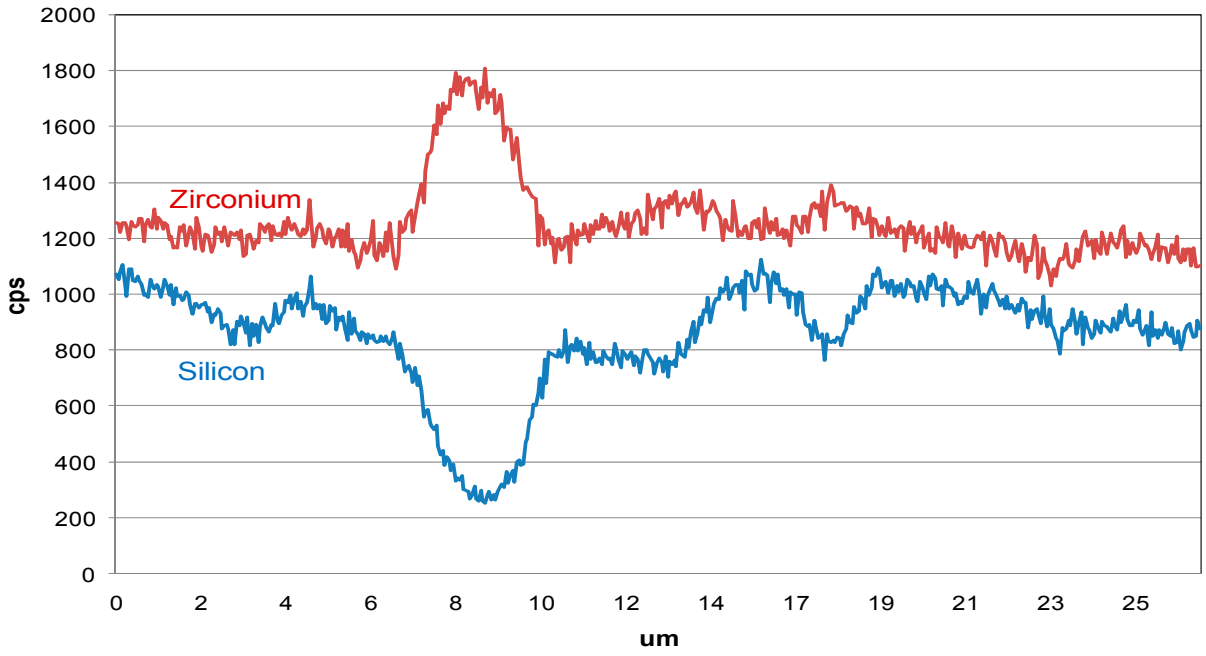

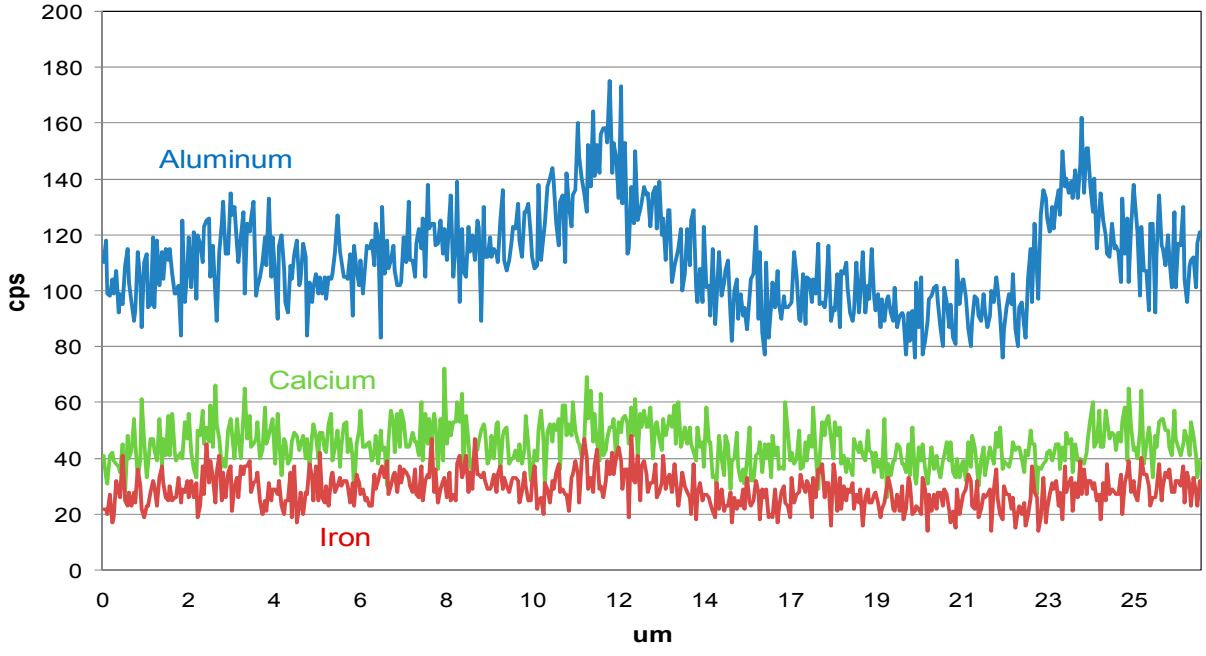

Thin section 512075
Zircon area 1

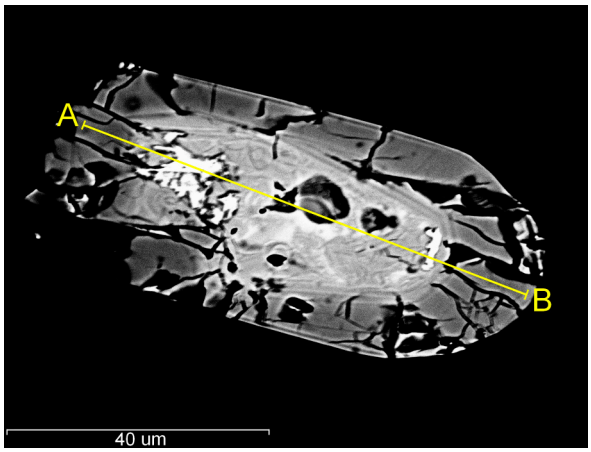

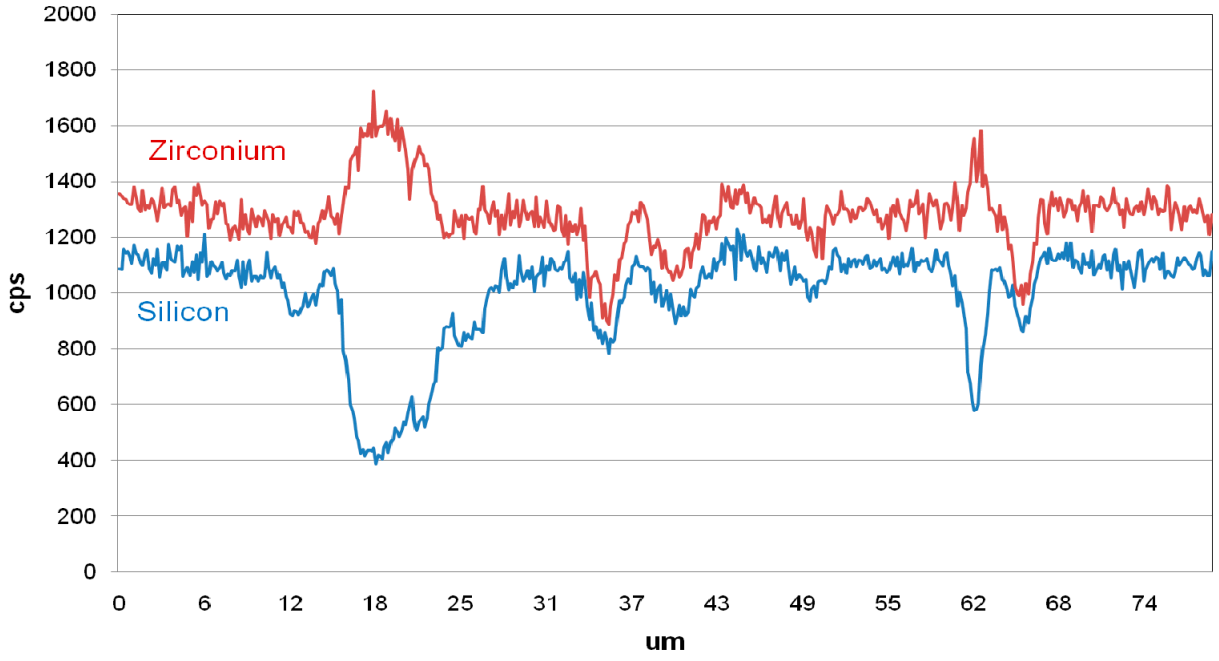

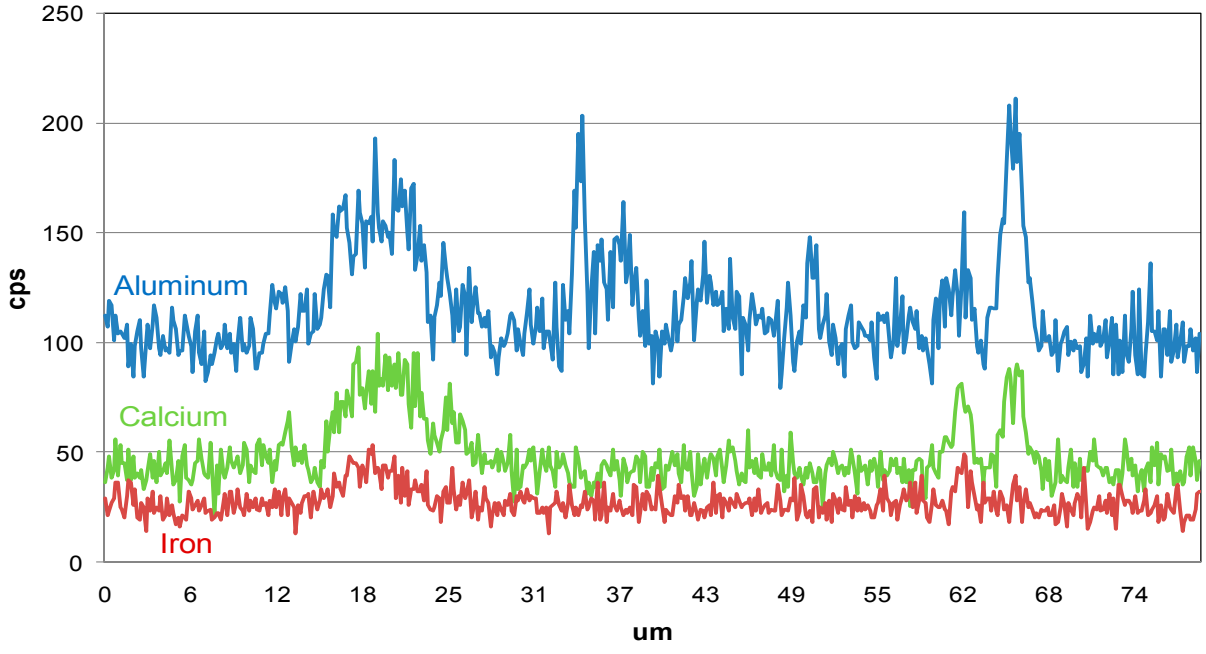

Appendix 4: Geochemical data

CIPW-norm

Norm mineral (%)	510155	512013	512028	512075
Qtz	30,9	37,5	27,3	43,0
Crn	0,87	0,86	0,21	1,17
Or	12,2	27,1	16,9	22,2
Ab	41,0	22,3	35,6	18,5
An	11,0	8,59	13,7	13,0
Hy	1,12	1,44	2,09	0,45
Ilm	0,04	0,04	0,09	0,02
Hem	1,52	1,29	2,70	0,43
Rt	0,18	0,13	0,31	0,04
Ap	0,17	0,14	0,28	0,05
Sum	99,2	99,4	99,3	98,9

Zircon saturation temperature

Sample	510155	512013	512028	512075
T/°C	745	766,8	745	764,8

Tidigare skrifter i serien ”Examensarbeten i Geologi vid Lunds Universitet”:

211. Nilsson, Pernilla, 2007: Kvidingedeltat – bildningsprocesser och arkitektonisk uppbyggnadsmodell av ett glacifluvialt Gilbertdelta.
212. Ellingsgaard, Óluva, 2007: Evaluation of wireline well logs from the borehole Kyrkheddinge-4 by comparsion to measured core data.
213. Åkerman, Jonas, 2007. Borrkärnekartering av en Zn-Ag-Pb-mineralisering vid Stenbrånet, Västerbotten.
214. Kurlovich, Dzmitry, 2007: The Polotsk-Kurzeme and the Småland-Blekinge Deformation Zones of the East European Craton: geomorphology, architecture of the sedimentary cover and the crystalline basement.
215. Mikkelsen, Angelica, 2007: Relationer mellan grundvattenmagasin och geologiska strukturer i samband med tunnelborrning genom Hallandsås, Skåne.
216. Trondman, Anna-Kari, 2007: Stratigraphic studies of a Holocene sequence from Taniente Palet bog, Isla de los Estados, South America.
217. Månsson, Carl-Henrik & Siikanen, Jonas, 2007: Measuring techniques of Induced Polarization regarding data quality with an application on a test-site in Aarhus, Denmark and the tunnel construction at the Hallandsås Horst, Sweden.
218. Ohlsson, Erika, 2007: Classification of stony meteorites from north-west Africa and the Dhofar desert region in Oman.
219. Åkesson, Maria, 2008: Mud volcanoes - a review. (15 hskp)
220. Randsalu, Linda, 2008: Holocene relative sea-level changes in the Tasiusaq area, southern Greenland, with focus on the Ta1 and Ta3 basins. (30 hskp)
221. Fredh, Daniel, 2008: Holocene relative sea-level changes in the Tasiusaq area, southern Greenland, with focus on the Ta4 basin. (30 hskp)
222. Anjar, Johanna, 2008: A sedimentological and stratigraphical study of Weichselian sediments in the Tvärkroken gravel pit, Idre, west-central Sweden. (30 hskp)
223. Stefanowicz, Sissa, 2008: Palynostratigraphy and palaeoclimatic analysis of the Lower - Middle Jurassic (Pliensbachian - Bathonian) of the Inner Hebrides, NW Scotland. (15 hskp)
224. Holm, Sanna, 2008: Variations in impactor flux to the Moon and Earth after 3.85 Ga. (15 hskp)
225. Bjärnborg, Karolina, 2008: Internal structures in detrital zircons from Hamrånge: a study of cathodoluminescence and back-scattered electron images. (15 hskp)
226. Noresten, Barbro, 2008: A reconstruction of subglacial processes based on a classification of erosional forms at Ramsvikslandet, SW Sweden. (30 hskp)
227. Mehlqvist, Kristina, 2008: En mellanjurassisk flora från Bagå-formationen, Bornholm. (15 hskp)
228. Lindvall, Hanna, 2008: Kortvariga effekter av tefranedfall i lakustrin och terrestrisk miljö. (15 hskp)
229. Löfroth, Elin, 2008: Are solar activity and cosmic rays important factors behind climate change? (15 hskp)
230. Damberg, Lisa, 2008: Pyrit som källa för spårämnen – kalkstenar från övre och mellersta Danien, Skåne. (15 hskp)
331. Cegrell, Miriam & Mårtensson, Jimmy, 2008: Resistivity and IP measurements at the Bolmen Tunnel and Ådalsbanan, Sweden. (30 hskp)
232. Vang, Ina, 2008: Skarn minerals and geological structures at Kalkheia, Kristiansand, southern Norway. (15 hskp)
233. Arvidsson, Kristina, 2008: Vegetationen i Skandinavien under Eem och Weichsel samt fallstudie i submoräna organiska avlagringar från Nybygget, Småland. (15 hskp)
234. Persson, Jonas, 2008: An environmental magnetic study of a marine sediment core from Disko Bugt, West Greenland: implications for ocean current variability. (30 hskp)
235. Holm, Sanna, 2008: Titanium- and chromium-rich opaque minerals in condensed sediments: chondritic, lunar and terrestrial origins. (30 hskp)
236. Bohlin, Erik & Landen, Ludvig, 2008: Geofysiska mätmetoder för prospektering till ballastmaterial. (30 hskp)
237. Brodén, Olof, 2008: Primär och sekundär

migration av hydrokarboner. (15 hskp)

238. Bergman, Bo, 2009: Geofysiska analyser (stångslingram, CVES och IP) av lagerföljd och lakvattenrörelser vid Albäcksdeponin, Trelleborg. (30 hskp)
239. Mehlqvist, Kristina, 2009: The spore record of early land plants from upper Silurian strata in Klinta 1 well, Skåne, Sweden. (45 hskp)
239. Mehlqvist, Kristina, 2009: The spore record of early land plants from upper Silurian strata in Klinta 1 well, Skåne, Sweden. (45 hskp)
240. Bjärnborg, Karolina, 2009: The copper sulphide mineralization of the Zinkgruvan deposit, Bergslagen, Sweden. (45 hskp)
241. Stenberg, Li, 2009: Historiska kartor som hjälp vid jordartsgeologisk kartering – en pilotstudie från Vångs by i Blekinge. (15 hskp)
242. Nilsson, Mimmi, 2009: Robust U-Pb baddeleyite ages of mafic dykes and intrusions in southern West Greenland: constraints on the coherency of crustal blocks of the North Atlantic Craton. (30 hskp)
243. Hult, Elin, 2009: Oligocene to middle Miocene sediments from ODP leg 159, site 959 offshore Ivory Coast, equatorial West Africa. (15 hskp)
244. Olsson, Håkan, 2009: Climate archives and the Late Ordovician Boda Event. (15 hskp)
245. Wollein Waldetoft, Kristofer, 2009: Svekofennisk granit från olika metamorfa miljöer. (15 hskp)
246. Månsby, Urban, 2009: Late Cretaceous coprolites from the Kristianstad Basin, southern Sweden. (15 hskp)
247. MacGimpsey, I., 2008: Petroleum Geology of the Barents Sea. (15 hskp)
248. Jäckel, O., 2009: Comparison between two sediment X-ray Fluorescence records of the Late Holocene from Disko Bugt, West Greenland; Paleoclimatic and methodological implications. (45 hskp)
249. Andersen, Christine, 2009: The mineral composition of the Burkland Cu-sulphide deposit at Zinkgruvan, Sweden – a supplementary study. (15 hskp)
250. Riebe, My, 2009: Spinel group minerals in carbonaceous and ordinary chondrites. (15 hskp)
251. Nilsson, Filip, 2009: Föroreningsspridning och geologi vid Filborna i Helsingborg. (30 hskp)
252. Peetz, Romina, 2009: A geochemical characterization of the lower part of the Miocene shield-building lavas on Gran Canaria. (45 hskp)
253. Maria Åkesson, 2010: Mass movements as contamination carriers in surface water systems – Swedish experiences and risks.
254. Elin Löfroth, 2010: Elin Löfroth, 2010: A Greeland ice core perspective on the dating of the Late Bronze Age Santorini eruption. (45 hskp)
255. Óluva Ellingsgaard, 2009: Formation Evaluation of Interlava Volcaniclastic Rocks from the Faroe Islands and the Faroe-Shetland Basin. (45 hskp)
256. Arvidsson, Kristina, 2010: Geophysical and hydrogeological survey in a part of the Nhandugue River valley, Gorongosa National Park, Mozambique. (45 hskp)
257. Gren, Johan, 2010: Osteo-histology of Mesozoic marine tetrapods – implications for longevity, growth strategies and growth rates. (15 hskp)
258. Syversen, Fredrikke, 2010: Late Jurassic deposits in the Troll field. (15 hskp)
259. Andersson, Pontus, 2010: Hydrogeological investigation for the PEGASUS project, southern Skåne, Sweden. (30 hskp)
260. Noor, Amir, 2010: Upper Ordovician through lowermost Silurian stratigraphy and facies of the Borenshult-1 core, Östergötland, Sweden. (45 hskp)
261. Lewerentz, Alexander, 2010: On the occurrence of baddeleyite in zircon in silica-saturated rocks. (15 hskp)

LUNDS UNIVERSITET

Geologiska enheten
Institutionen för geo- och ekosystemvetenskaper
Sölvegatan 12, 223 62 Lund